GEOLOGICA CARPATHICA, FEBRUARY 2015, 66, 1, 19–36 doi: 10.1515/geoca-2015-0008

Intensive low-temperature tectono-hydrothermal overprint of peraluminous rare-metal granite: a case study from the Dlhá dolina valley (Gemericum, Slovakia)

KAREL BREITER[1], IGOR BROSKA[2] and PAVEL UHER[3]

[1]Institute of Geology, Czech Academy of Sciences, v.v.i., Rozvojová 269, CZ-16500 Praha 6, Czech Republic; breiter@gli.cas.cz
[2]Geological Institute of the Slovak Academy of Sciences, Dúbravská 9, 840 05 Bratislava, Slovak Republic; geolbros@savba.sk
[3]Department of Mineralogy and Petrology, Faculty of Natural Sciences, Comenius University, Mlynská dolina G, 842 15 Bratislava, Slovak Republic; puher@fns.uniba.sk

(Manuscript received June 4, 2014; accepted in revised form December 10, 2014)

Abstract: A unique case of low-temperature metamorphic (hydrothermal) overprint of peraluminous, highly evolved rare-metal S-type granite is described. The hidden Dlhá dolina granite pluton of Permian age (Western Carpathians, eastern Slovakia) is composed of barren biotite granite, mineralized Li-mica granite and albitite. Based on whole-rock chemical data and evaluation of compositional variations of rock-forming and accessory minerals (Rb-P-enriched K-feldspar and albite; biotite, zinnwaldite and di-octahedral micas; Hf-(Sc)-rich zircon, fluorapatite, topaz, schorlitic tourmaline), the following evolutionary scenario is proposed: (1) Intrusion of evolved peraluminous melt enriched in Li, B, P, F, Sn, Nb, Ta, and W took place followed by intrusion of a large body of biotite granites into Paleozoic metapelites and metarhyolite tuffs; (2) The highly evolved melt differentiated in situ forming tourmaline-bearing Li-biotite granite at the bottom, topaz-zinnwaldite granite in the middle, and quartz albitite to albitite at the top of the cupola. The main part of the Sn, Nb, and Ta crystallized from the melt as disseminated cassiterite and Nb-Ta oxide minerals within the albitite, while disseminated wolframite appears mainly within the topaz-zinnwaldite granite. The fluid separated from the last portion of crystallized magma caused small scale greisenization of the albitite; (3) Alpine (Cretaceous) thrusting strongly tectonized and mylonitized the upper part of the pluton. Hydrothermal low-temperature fluids enriched in Ca, Mg, and CO_2 unfiltered mechanically damaged granite. This fluid-driven overprint caused formation of carbonate veinlets, alteration and release of phosphorus from crystal lattice of feldspars and Li from micas, precipitating secondary Sr-enriched apatite and Mg-rich micas. Consequently, all bulk-rock and mineral markers were reset and now represent the *P-T* conditions of the Alpine overprint.

Key words: rare-metal granite, low-temperature overprint, Western Carpathians, Slovakia.

Introduction

Huge number of ore-bearing granitic systems of different geochemical types (S-, A-, I-type) have been described through the world and many genetic models and strategies for the detection of hidden Sn-W and Ta-bearing mineral deposits were proposed (Beus & Zalashkova 1962; Koval 1975; Kovalenko & Kovalenko 1976; Frolov 1978; Taylor & Strong 1985; Tischendorf et al. 1989; Lehmann 1990; Štemprok 1993; Seltmann et al. 1994; Štemprok et al. 1994; Haapala 1995; Breiter et al. 1999; Jarchovský 2004; Bastos Neto et al. 2009; Küster 2009; Solomovich et al. 2012). The majority of ore-bearing objects examined in detail are preserved in their "primary" high-temperature magmatic to early hydrothermal stage which involves magmatic crystallization and the complex of immediately following relatively high-temperature "autometasomatic" processes, like feldspatization and greisenization. Sn-W granite-related mineral deposits/occurrences which underwent HP–HT (high pressure–high temperature) regional metamorphism have only rarely been described. The examples include Cetoraz (Němec & Páša 1986) and Kovářová near Nedvědice (Losos & Vižda 2006), both in the Moldanubian block of the Bohemian Massif, Czech Republic.

In this study, a unique case of LT (low-temperature) metamorphic (tectono-hydrothermal) overprint of ore-bearing Li, P, F, Sn, W, Nb, Ta-rich, rare-metal S-type granite is described. The hidden Permian granite occurring in the Dlhá dolina valley (Western Carpathians, Gemeric Superunit, eastern Slovakia) underwent intensive Alpine (Cretaceous) overprint (Radvanec et al. 2004; Petrasová et al. 2007). However, the chemical composition of the rock-forming and indicative accessory minerals from the Li-bearing granites discovered by drilling in 1980 located in Dlhá dolina are still insufficiently characterized (Dianiška et al. 2002). The neighbouring Li-bearing granites from the Surovec body and Vrchsúľová contain Li-rich phengitic mica which was formed during Alpine metamorphism from primary zinnwaldite series and muscovite (Petrík et al. 2014). We evaluate compositional variations of the rock-forming and accessory minerals in the context of bulk-rock vertical chemical zoning of the Dlhá dolina granite body, in comparison with a wide range of world-wide rare-metal granites, as important potential sources of critical metals, such as Sn, Nb, Ta, Li and W.

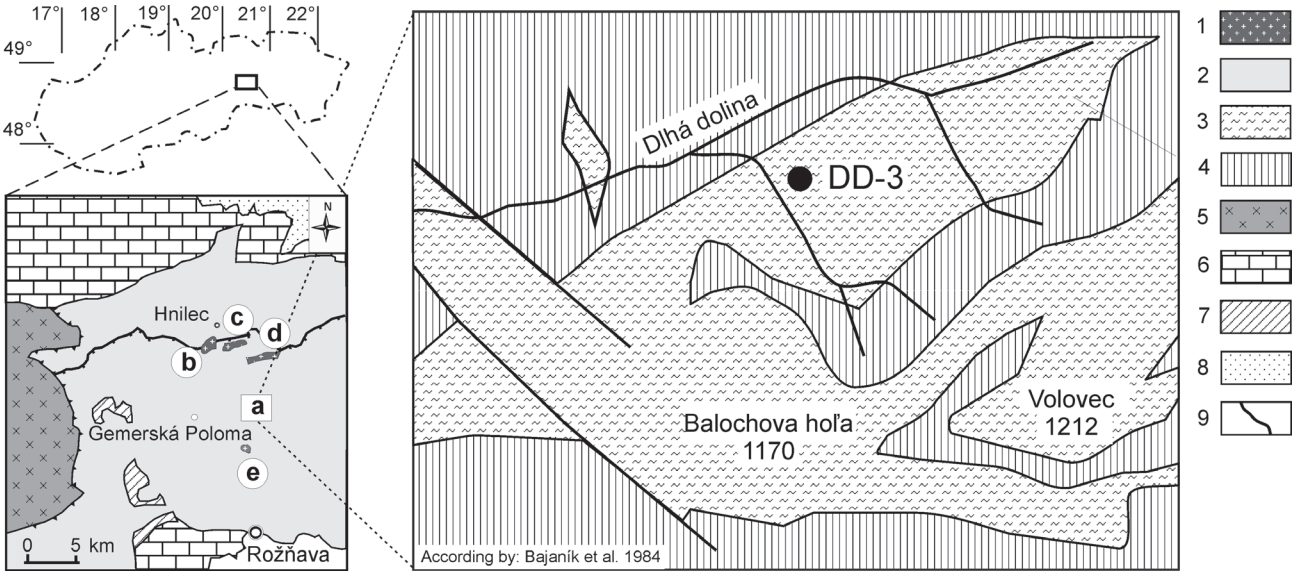

Fig. 1. Simplified map of the studied area. **1** — specialized S-type granite bodies (a — Podsúľová, b — Hnilec, c — Delava, d — Surovec, e — Betliar), **2** — undistinguished Paleozoic metamorphic rocks of the Gemeric Superunit (phyllites, metasandstones, metavolcanics), **3** — metarhyolite tuffs, **4** — phyllites, **5** — Veporicum (paragneisses, granitoids), **6** — Silicicum (limestone, dolomite; Lower Triassic to Upper Jurassic), **7** — Meliaticum (Late Permian to Upper Jurassic), **8** — Sediments of Inner Carpathians, **9** — Quaternary sediments with streams.

Geological setting and sampling

Geological background

Within the Western Carpathians, the rare-metal granites are developed only in the Gemeric Superunit as co-called specialized S-type granites due to their special ore-bearing, Li-Sn-W-Nb-Ta mineralization (Uher & Broska 1996). The first outcrop of tin mineralization in the granites was detected near the Hnilec village (e.g. Baran et al. 1970, 1971; Drnzíková et al. 1975). Hidden P, F, Li, Nb, Ta, Sn-rich granite represents a strongly fractionated small granite pluton composed of barren biotite granite, mineralized Li-mica granite and albitite. The granite was discovered in the Dlhá dolina valley close to the village of Gemerská Poloma (Fig. 1) on the basis of heavy mineral prospection (Tréger & Matula 1977). About twenty inclined exploration boreholes were realized to recognize the shape and composition of the pluton (Malachovský et al. 1983, 1992). Among them, the 912.9 m long hole DD-3 was the deepest and this work describes the main geochemical findings from this drillhole.

The Dlhá dolina pluton was emplaced within the intensively folded Lower Paleozoic volcano-sedimentary complex of the Vlachovo Formation, metamorphosed in the greenschist-facies during Variscan orogeny (Carboniferous). Moreover, the granites and metamorphic rocks were overprinted by Alpine (Cretaceous) regional metamorphism, which reached ~600 to 700 MPa and ~400 °C (Petrasová et al. 2007). The country rocks composed mainly of phyllites, metarhyolites and their metapyroclastic equivalents as well as layers or lenses of coarse-grained metadolomites and strongly steatitized magnesites with a talc deposit near Gemerská Poloma (Kilík 1997; Petrasová et al. 2007; Vozárová et al. 2010). The U-Pb SHRIMP dating of zircon from the metamorphosed rhyolitic rocks of the Vlachovo Formation gave Late Cambrian age (494 ± 1.6 Ma — Vozárová et al. 2010). According to the drilling survey (Malachovský et al. 1992), the hidden Dlhá dolina granite pluton forms a NE-SW

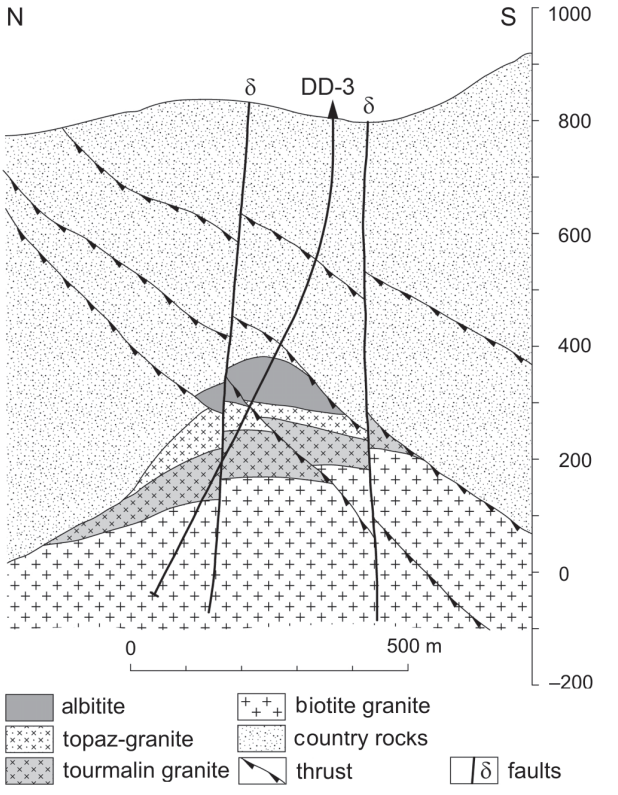

Fig. 2. Cross-section through the borehole DD-3, in the Dlhá dolina pluton (acc. to Malachovský et al. 1992, strongly modified).

oriented, 2 km long and 200 to 1000 m wide granite body (dimensions at sea level). The actual shape of the pluton is determined through multiple NE-SW trending, to the SE inclined, local Alpine thrusting. The original upper contact of the pluton was probably generally flat with two cupolas with diameters of about 500 m rising about 200 m above the entire pluton. The SW-cupola, cut by the borehole DD-3 (Fig. 2), had more steep contacts and its upper part was filled by albitite, while within the more flat-shaped NE cupola only mild greisenization took place (Malachovský et al. 1992).

The age of the granite intrusion is probably similar to that of the nearest outcropping Hnilec granite body, which is interpreted on the basis of zircon U-Pb dating of granites (Poller et al. 2002) and Re-Os in molybdenite dating of Sn-W-Mo mineralization (Kohút & Stein 2005) as Late Permian (~260 to 250 Ma)

Sampling and description of granites

We studied samples from the core of the deepest DD-3 borehole located in the Dlhá dolina valley at an altitude of 800 m above see level, 1.8 km to the NW from the Volovec hill (1212 m a.s.l.) (Fig. 1). Each sample for chemical analysis (Table 1) consisted of several fragments (2–6 pieces, 3–5 kg in the whole) from the macroscopically homogeneous section of the core. Polished thin sections were prepared from the most typical rock pieces.

The pluton is composed of two co-magmatic constituents: the deeper suite of barren biotite granites, and the upper suite of highly fractionated, rare-metal Li-mica granites and quartz albitite. While the deeper suite probably forms a larger body with generally flat upper contact, the upper suite forms cupola-like bodies with steep contacts located between the deeper suite and its metamorphic envelope. Alpine (Cretaceous) tectonic processes (thrusting, mylonitization) affected the whole pluton, but the intensity of deformation is highly variable. Generally, the intensity of deformation increases upwards. Intact rocks, namely granites unaffected by deformation and/or metasomatism, are preserved only in the centers of large tectonic blocks. Rocks from the depth of 681 to 691 m (tourmaline granite), 577 to 582 m (topaz granite) and 459 to 461 m (quartz albitite) can best represent the primary magmatic stage of this system. The principal granite types from the deepest to the apical part of the cupola have the following succession:

The deeper intrusive suite (biotite granites)

(1) *Distinctly porphyritic biotite granite* in the depth of 880 to 913 m is grey coloured, composed of phenocrysts of K-feldspars (up to 3 cm) and quartz (up to 1 cm) in fine-grained groundmass of K-feldspar, albite (An_{06}), quartz, and biotite, mostly altered to a mixture of chlorite and phengitic mica. Zircon, apatite, ilmenite, rutile and tourmaline are characteristic accessory mineral phases. Many tectonic planes are covered by secondary chlorite and phengitic muscovite.

(2) *Slightly porphyritic biotite granite* in the depth of 720 to 880 m is pink-coloured and composed of phenocrysts of twinned K-feldspars (up to 15 mm) and quartz (up to 8 mm) in medium-grained groundmass consisting of subhedral K-feldspar, albite (An_{08}), quartz and partly chloritized biotite. The typical accessory minerals comprise apatite, zircon, schorlitic tourmaline and almandine garnet.

The upper intrusive suite (Li-mica granites)

(3) *Li-biotite granite with tourmaline (hereinafter tourmaline granite)* forms the lower part of the ore-bearing intrusion in the depth of 620 to 720 m. This is grey, coarse to medium grained (3–8 mm) leucogranite, composed of albite (An_{04}), K-feldspar, quartz and Li-Fe mica. Black tourmaline (schorl) forms common disseminated grains (< 1 mm) and occasionally aggregates up to 15 mm in size. The K-feldspar locally forms phenocrysts up to 12 mm in size. Accessory phases are apatite, zircon, monazite, xenotime, wolframite, wolframixiolite, columbite, cassiterite, uraninite, thorite, goyazite, fluorite, etc. Upwards the tourmaline granite gradually changed into topaz granite.

(4) *Zinnwaldite granite with topaz (hereafter topaz granite)* forms the medium part of the intrusion at the depth of 554 to 620 m. This part of the granite cupola was affected with strong deformation and metasomatism and only the domain at the depth of ca. 575 to 590 m is preserved in a nearly primary shape. The granite is light grey to white in colour, fine- to medium-grained and leucocratic, composed of albite (An_{02}), P-enriched K-feldspar, snow-ball textured quartz, and zinnwaldite. Zircon, apatite, fluorite, monazite, xenotime, Nb-rich wolframite (mainly ferberite), columbite-group minerals, W-rich ixiolite-like phase, ilmenite, cassiterite, uraninite, and Bi-sulfosalts occur among the accessory minerals. Some discontinuity planes are coated with fluorite. The uppermost part of this unit (in depth of 555 to 575 m) is strongly mylonitized.

(5) *Quartz albitite to albitite (hereinafter albitite)* forms the uppermost part of the cupola at the depth of 454 to 554 m. This rock type is usually hololeucocratic, fine- to medium-grained, composed of albite (An_{01}), quartz and K-feldspar in highly variable amounts (Ab > Qtz > > Kfs). The modal content of albite varies in the range 50–90 vol. %, mostly 70–90 vol. %. In some parts, apatite and/or muscovite are present as major constituents. Intercalations of K-feldspar- and mica-enriched facies in the depth of 490 to 495 m approach the composition of topaz granite. Some parts of the albitite body were silicified and these quartz (+apatite) enriched domains were originally described as "greisens" (Malachovský et al. 1992). The genesis of these quartz-rich rock and real extension of high-temperature metasomatism (=greisenization) remains questionable, due to strong mylonitization. In zones of intensive mylonitization, feldspars were replaced by a young generation of quartz and phengitic mica. Disseminated cassiterite, Nb-Ta oxide minerals (ferrocolumbite to manganocolumbite, Nb-Ta-rich rutile) and U-phases (uraninite, brannerite) were found through the whole albitite body without specific relation to the silicified areas.

Table 1: Studied samples from the borehole DD-3 Dlhá dolina.

Sample No.	Depth (m)	Unit	Description
3626	459.0–461.6	Upper intrusive suite, albitites	Quartz albitite
3627	471.2–473.4		Slightly silicified albitite
3628	487.0–489.0		Strongly silicified (greisenized) and mylonitized albitite
3629	489.0–490.5		Apatite-rich albitite
3630	504.2–507.7		Mylonitized albitite
3631	559.0–561.7	Upper intrusive suite, Li-mica granites	Mylonitized topaz granite
3632	569.8–574.0		Mylonitized topaz granite
3633	577.4–582.4		Topaz granite, without alteration
3634	594.9–597.8		Mylonitized topaz granite
3635	607.9–611.4		Mildly mylonitized topaz granite
3636	627.4–633.9		Sericitized tourmaline granite
3637	657.9–664.0		Sericitized tourmaline granite
3638	681.6–691.5		Tourmaline granite
3639	783.3–787.7	Deeper intrusive suite, biotite granites	Biotite granite
3640	870.2–873.8		Biotite granite
3641	908.2–910.9		Porphyritic biotite granite

Analytical methods

Whole-rock analyses

The major element analyses were performed by wet technique at the Czech Geological Survey, Praha. The control analyses of the international whole-rock reference materials yield a total error (1-sigma) of ±0.5 %. Trace element analyses were obtained in the ACME Labs, Vancouver, using ICP-MS method after melting with lithium borate.

Cathodoluminescence (CL)

The CL images of the selected samples were obtained using a microscope HC2-LM (Lumic), accelerating voltage 14 kV, and current density 10–40 μA/mm^2. The images were captured with an Olympus C-5060 digital camera (setting: ISO 400, exposure time 1–10 sec) at the Department of Geological Sciences, Masaryk University, Brno, Czech Republic.

EMPA analyses of minerals

Silicate minerals and apatite were analysed using a CAMECA SX100 electron microprobe in the Geological Institute, Czech Academy of Science in Praha, at an accelerating voltage and beam current of 15 kV and 10 nA, respectively, and with a beam diameter 2 μm. The following standards were used: P — apatite, Si, Mg, Ca — diopside, Ti — rutile, Al, Na, — jadeite, Fe — magnetite, Mn — $MnCr_2O_4$, Ba — $BaSO_4$, K — leucite, Rb — RbCl and F — fluorite.

Zircon was analysed using a CAMECA SX100 electron microprobe at the Dionýz Štúr State Geological Institute, Bratislava, using accelerating voltage of 15 kV and sample current of 40 nA. The following standards were used for calibration: P and Ca — apatite, As–GaAs, Nb — ferrocolumbite, Si and Zr — zircon, Hf–HfO_2, Th–ThO_2, U–UO_2, Al–Al_2O_3 Sc–$ScPO_4$, Y–YPO_4, La–$LaPO_4$, Ce–$CePO_4$, Pr–$PrPO_4$, Nd–$NdPO_4$, Sm–$SmPO_4$, Eu–$EuPO_4$, Gd–$GdPO_4$, Tb–$TbPO_4$, Dy–$DyPO_4$, Ho–$HoPO_4$, Er–$ErPO_4$, Tm–$TmPO_4$, Yb–$YbPO_4$, Lu–$LuPO_4$, Fe — fayalite, and Mn — rhodonite. We used empirically determined correction factors applied to the following line overlaps: Th→U, Dy→Eu, Gd→Ho, La→Gd, Ce→Gd, Eu→Er, Gd→Er, Sm→Tm, Dy→Lu, Ho→Lu, Yb→Lu, and Dy→As. The matrix effects were corrected using the PAP procedure.

Whole-rock geochemistry

Typical whole-rock chemical analyses are shown in Table 2. Contents of some elements and their relations are visualized in Fig. 3.

Both intrusive suites have different geochemical characteristics. The lower suite of biotite granites, although variable in texture, is chemically homogeneous. It is slightly peraluminous (ASI=1.1) and alkaline (75.0–75.6 wt. % SiO_2, 12.2–13.1 wt. % Al_2O_3, 0.6 wt. % CaO, 2.8–3.2 wt. % Na_2O, 4.8–5.3 wt. % K_2O) with low contents of fluxing elements (about 0.01 wt. % Li_2O, 0.12–0.14 wt. % P_2O_5, 0.2 wt. % F). The contents of trace elements (425–459 ppm Rb, 20–31 ppm Sr, 10–11 ppm Nb, 24–30 ppm Sn, 73–93 ppm Zr, 21–30 ppm Ce and 24–30 ppm Y) are comparable with other biotite and two-mica granites in the Gemeric Superunit, especially in its western part (Hnilec area — Broska & Uher 2001).

The upper ore-bearing intrusive suite as a whole shows a much higher grade of geochemical specialization. In comparison with the foregoing biotite granites, the Li-mica granites are depleted in Si, Ti, Fe, K, Zr, Y, REE, and enriched in Al, Na, Li, P, F, Cs, Ga, Nb, Rb, Sn, Ta, and W. The contents of Fe, Mg, Ca, Ba, Sr, U, and Th are scattered and strongly influenced by late processes. Going from the lower tourmaline- to the upper topaz-bearing facies, the content of Si decreases (73 to 71 wt. %), while contents of other index elements increase: P (0.3 to 0.6 wt. % P_2O_5), F (0.5 to 1.5 wt. % F), Li (0.05 to 0.3 wt. % Li_2O), Nb (22 to 63 ppm), and W (8 to 82 ppm).

Albitite in the uppermost part of the cupola is rich in Na (up to 9.4 wt. % Na_2O), Ga (ca. 50 ppm), Sn (400–900 ppm), Ta (40–95 ppm) and poor in K (0.5–1.8 wt. % K_2O), F (ca. 0.1 wt. %), and Rb (87–118 ppm). Secondary processes (silicification, mylonitization, sericitization, carbonatization) are

Table 2: Bulk-rock chemical analyzes of studied granitoids (wt. %, trace elements in ppm).

Rock	Quartz albitite	Silicified and mylonitized albitite	Mylonitized topaz granite	Topaz granite	Tourmaline granite	Biotite granite	Porphyritic biotite granite
Sample	**3626**	**3628**	**3631**	**3633**	**3638**	**3640**	**3641**
SiO_2	72.81	79.69	69.21	71.68	73.24	74.96	75.57
TiO_2	0.01	0.02	0.02	0.03	0.06	0.10	0.14
Al_2O_3	15.80	11.33	16.30	15.66	14.11	13.06	12.21
Fe_2O_3	0.05	0.263	0.27	0.18	0.46	0.44	0.82
FeO	0.09	0.33	0.45	0.51	0.58	0.83	1.19
MnO	0.005	0.021	0.037	0.050	0.022	0.037	0.056
MgO	0.14	0.66	1.66	0.02	0.26	0.16	0.18
CaO	0.43	0.87	1.81	0.72	0.70	0.56	0.56
Li_2O	0.005	0.018	0.021	0.282	0.050	0.010	0.012
Na_2O	9.37	0.92	1.54	4.13	3.57	3.22	2.85
K_2O	0.61	3.46	4.94	4.36	4.66	5.26	4.87
P_2O_5	0.30	0.52	0.45	0.49	0.27	0.12	0.12
F	0.08	0.31	0.29	1.38	0.48	0.18	0.21
LOI	0.46	1.74	3.41	1.15	1.08	0.92	0.89
$H_2O–$	0.04	0.06	0.07	0.05	0.06	0.03	0.04
Total	100.17	100.08	100.35	100.11	99.4	99.81	99.62
ASI	0.94	1.66	1.46	1.22	1.16	1.09	1.11
Nb/Ta	1.0	1.4	2.9	3.3	2.9	4.0	4.8
Zr/Hf	6.3	6.0	9.0	10.5	19.9	24.5	28.2
Ba	15	47	40	58	96	84	81
Be	1	2	2	2	6	7	6
Cs	3.9	26	51	74	52	14	20
Ga	51	25	45	40	27	20	20
Hf	4.8	4.5	2.7	2.4	2.9	3	3.3
Nb	70	138	83	601	22	9.7	10
Rb	100	744	1209	1698	802	459	436
Sn	654	926	198	92	57	25	24
Sr	52	118	57	187	24	20	22
Ta	71	96	29	189	7.6	2.4	2.1
Th	6.5	8.2	6.9	9.4	11	14	15
U	21	26	24	24	26	17	19
W	4.3	13	8	82	8.4	6.1	5.5
Zr	30	27	24	25	58	73	93
Y	0.4	1.3	2.3	5	17	24	30
La	0.2	0.5	1.2	0.6	5.4	9.2	12.9
Ce	0.4	0.9	2.5	2.1	12.3	21.4	30.2
Pr	0.06	0.14	0.31	0.31	1.53	2.59	3.67
Nd	<0.3	0.6	1.2	1.3	5.5	8.9	13.4
Sm	0.09	0.29	0.45	0.69	1.84	2.6	3.44
Eu	0.05	0.08	0.16	<0.02	0.07	0.15	0.2
Gd	0.11	0.38	0.41	0.6	1.96	2.65	3.6
Tb	0.02	0.07	0.08	0.19	0.5	0.62	0.81
Dy	0.08	0.31	0.36	0.93	3.18	4.09	5.26
Ho	<0.02	0.05	0.05	0.12	0.58	0.84	1.09
Er	0.04	0.12	0.17	0.36	1.63	2.61	3.24
Tm	<0.01	0.02	0.03	0.07	0.27	0.44	0.52
Yb	<0.05	0.1	0.28	0.56	1.71	3.04	3.49
Lu	<0.01	0.02	0.04	0.07	0.23	0.44	0.49

responsible for local increase of Si (up to 79.7 wt. % SiO_2), Mg (up to 0.87 wt. % MgO), Ca (up to 1.37 wt. % CaO), P (up to 0.80 wt. % P_2O_5), and Sr (up to 153 ppm).

Mineralogy

Feldspars

Biotite granites contain perthitic K-feldspar (Ab_{04}, max. 0.14 wt. % BaO, Rb-free) in association with slightly zoned altered albite (An_{03-08}). The K-feldspar is locally enriched in phosphorus (max. 0.4 wt. % P_2O_5, 0.015 apfu P), while albite is P-free (Table 3).

Li-mica granites contain pure albite (An_{00-01}) and Ba-free perthitic K-feldspar (Ab_{02}). The content of Rb in Kfs increases upwards from 0.1 wt. % Rb_2O in tourmaline granite to ca. 0.4 wt. % Rb_2O (0.013 apfu Rb) in topaz granite and is not influenced by the low-temperature alteration. In contrast, the primary high content of phosphorus in both feldspars is preserved only rarely in the core of some grains (up to 0.54 wt. % P_2O_5 in Kfs and 0.30 wt. % P_2O_5 in albite). The majority of feldspar grains are actually P-free, but contain plenty of μm-sized inclusions of secondary apatite.

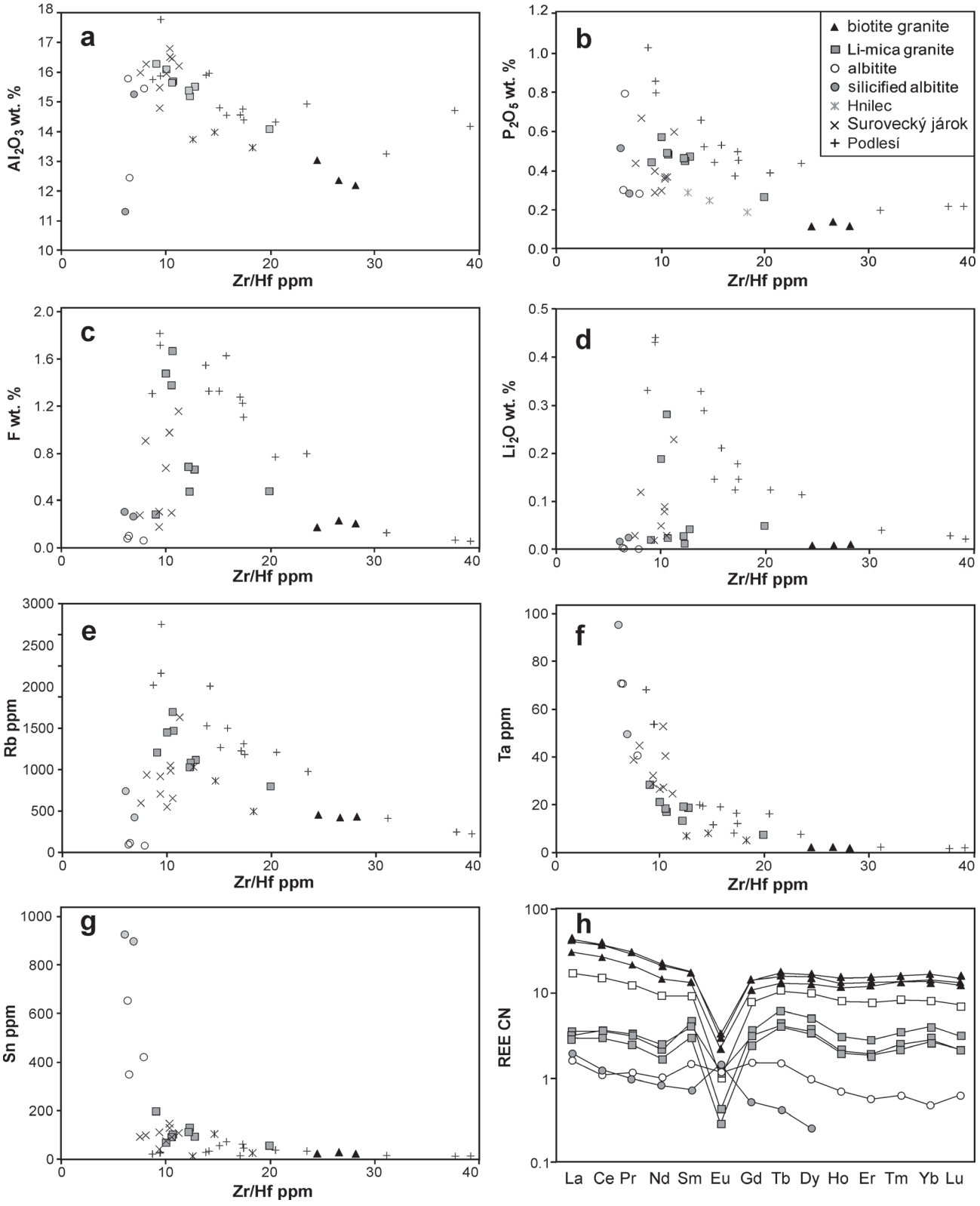

Fig. 3. Harker diagrams and chondrite normalized REE patterns of the Dlhá dolina granitic rocks. The atomic Zr/Hf-value (x-axis) is the most stable indicator of magma fractionation in the case of altered rocks. For comparison, representative analyses of Hnilec granites (unpublished data by I. Broska), Surovec granites (Petrík et al. 2011) and pure magmatic rare-metal granites from the Podlesí, western Krušné hory/Erzgebirge, Czech Republic (unpublished data by K. Breiter) are shown. **a** — Zr/Hf vs. Al_2O_3, **b** — Zr/Hf vs. P_2O_5, **c** — Zr/Hf vs. F, **d** — Zr/Hf vs. Li_2O, **e** — Zr/Hf vs. Rb, **f** — Zr/Hf vs. Ta, **g** — Zr/Hf vs. Sn, **h** — chondrite normalized REE patterns. HREE in the albitite are lower than the detection limits of ICP-MS. Chondrite values according to Mc Donough & Sun (1995).

Table 3: Representative compositions (in wt. %) and empirical formulae (based on 8 oxygen atoms) of alkali feldspars.

Sample	3626	3629	3633	3641	3641	3633	3633	3638	3641
Rock	Albitite	Mylonitized albitite	Topaz granite	Biotite granite	Biotite granite	Topaz granite	Topaz granite	Tourmaline granite	Biotite granite
Mineral	Albite	Albite	Albite	Albite core	Albite rim	K-feldspar	K-feldspar	K-feldspar	K-feldspar
SiO_2	68.74	68.16	67.08	64.11	67.45	64.13	63.67	63.43	63.24
TiO_2	<0.05	<0.05	0.01	0.01	<0.05	<0.05	<0.05	<0.05	<0.05
Al_2O_3	18.94	19.43	19.40	22.54	20.00	17.41	17.64	17.58	18.06
FeO	0.04	0.03	0.06	0.09	0.11	<0.05	0.08	<0.05	0.05
MgO	0.00	0.02	<0.05	0.03	<0.05	<0.05	<0.05	<0.05	0.02
MnO	0.00	0.07	<0.05	<0.05	<0.05	0.01	0.02	0.05	0.00
CaO	0.04	0.02	0.22	1.64	0.55	<0.05	<0.05	0.01	0.00
BaO	0.01	<0.05	<0.05	0.02	<0.05	<0.05	<0.05	0.03	0.14
Na_2O	11.99	12.20	11.74	10.40	11.70	0.32	0.20	0.28	0.34
K_2O	0.06	0.04	0.06	0.75	0.07	16.71	17.06	16.60	16.30
Rb_2O	<0.05	<0.05	<0.05	<0.05	<0.05	0.34	0.40	0.13	0.02
P_2O_5	0.40	0.03	0.40	<0.05	0.02	0.09	0.44	0.01	0.08
Total	100.23	100.05	98.97	99.58	99.93	99.01	99.51	98.12	98.25
Si	2.996	2.985	2.965	2.841	2.959	3.014	2.985	3.005	2.986
Ti	0.000	0.000	0.000	0.000	0.000	0.000	0.000	0.000	0.000
Al	0.973	1.003	1.010	1.177	1.034	0.965	0.975	0.982	1.005
Fe	0.001	0.001	0.002	0.003	0.004	0.000	0.003	0.000	0.002
Mg	0.000	0.001	0.000	0.002	0.000	0.000	0.000	0.000	0.002
Mn	0.000	0.002	0.000	0.000	0.000	0.000	0.001	0.002	0.000
Ca	0.002	0.001	0.011	0.078	0.026	0.000	0.000	0.000	0.000
Ba	0.000	0.000	0.000	0.000	0.000	0.000	0.000	0.001	0.003
Rb	0.000	0.000	0.000	0.000	0.000	0.010	0.012	0.004	0.001
Na	1.013	1.036	1.006	0.894	0.995	0.029	0.018	0.026	0.031
K	0.003	0.002	0.003	0.042	0.004	1.002	1.020	1.003	0.982
P	0.015	0.001	0.015	0.000	0.001	0.004	0.017	0.000	0.003

Albitite contains only pure albite ($An_{<01}$). Like the Li-mica granite, this albite equilibrated with hydrothermal fluids and contains numerous inclusions of secondary apatite. Some grain cores contain max. 0.4 wt. % P_2O_5 (0.015 apfu P).

Micas

Micas originated in all episodes of granite evolution: magmatic crystallization, high-temperature alteration (greisenization), and low-temperature Alpine overprint. The later processes have not only produced a new population of mica, but also re-equilibrated mica grains crystallized during the earlier episode, so the micas represent genetically the most complicated mineral group.

The most important signature of the magmatic micas is, along with their texture, relatively high contents of F, Li, and Rb. While it is not technically possible to analyse Li using the electron microprobe, high contents of F and Rb are the most important indicators of the magmatic origin of a particular mica. Biotite from the deeper intrusive suite is poor in Mg (#Mg 0.25–0.30) and Rb (0.10–0.14 wt. % Rb_2O) and free of fluorine (<0.1 wt. % F) (Fig. 4, Table 4). Associated Fe-dominant chlorite (chamosite) is relatively slightly Mg-depleted (#Mg 0.15) in comparison with the biotite.

In the whole body of tourmaline and topaz granites, only the sample from the depth of ca. 580 m contains mica, which can be considered as primary magmatic mica. This zinnwaldite forms typical bright brownish flakes 0.5 mm in size containing inclusions of zircon and ore minerals. The fresh cores are relatively rich in Fe (9.4 wt. % FeO, 1.15 apfu Fe), Rb (up to 1.5 wt. % Rb_2O, 0.14 apfu Rb) and F (up to 7.7 wt. % F, 3.7 apfu F), while slightly altered rims are enriched in Al (up to 24 wt. % Al_2O_3, 4.0 apfu Al) and depleted in all the afore mentioned elements (6.1–7.0 wt. % FeO, 0.13–0.78 wt. % Rb, 4.7–5.9 wt. % F). Contents of SiO_2 are scattered between 48.5–49.4 wt. % (7.0–7.4 apfu Si). Using the published equations for correlation between contents of Li and Si, Li-contents in the mica cores should be ca. 3.8–4.0 wt. % Li_2O (~2.2 apfu Li — Breiter et al. 2005) or 4.8–5.0 wt. % Li_2O (~2.7 apfu Li — Tischendorf et al. 1999). According to bulk-rock Li-contents, the lower values seem to be more realistic.

The micas from all other samples from the "Li-mica granites" are to variable degrees altered: enriched in Al (30–32 wt. % Al_2O_3), Mg (up to 1.9 wt. % MgO), and depleted in Fe (4.3 to 0.3 wt. % Fe), Rb (<0.3 wt. % Rb_2O), and F (<2.4 wt. % F). This mica should be termed as phengitic muscovite.

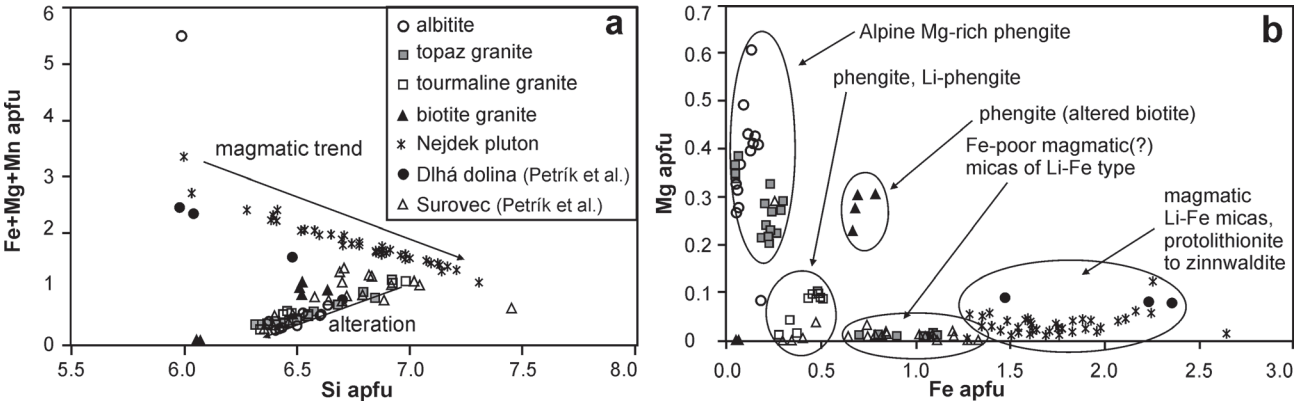

Fig. 4. Diagrams of mica composition (recalculated on the basis of 22 atoms of oxygen). **a** — Diagram Si vs. Fe+Mg+Mn shows different trends in magmatic micas from the Nejdek-Podlesí pluton, Czech Republic (unpublished data by K. Breiter) and low-temperature altered micas from the Dlhá dolina pluton. For comparison, published analyses of micas from near Surovec and Dlhá dolina granites (Petrík et al. 2011, 2014) are also shown. **b** — Diagram Fe vs. Mg in micas documents depletion in Fe and enrichment of Mg during Alpine LT alteration of the Dlhá dolina and Surovec granites. Rare phlogopite (4.0–4.5 apfu Mg) found in the mylonitized albitite do not match the field of this diagram. Remember, these diagrams are not IMA-classification diagrams of micas.

Zircon

It forms euhedral to subhedral crystals, usually 50 to 150 μm in size, scattered in quartz, albite and muscovite. The crystals are commonly partly to totally metamict, in some cases with tiny inclusions or intergrowths of xenotime-(Y), $ThSiO_4$ phase (thorianite or huttonite), uraninite, cassiterite, and (W)-Nb-Ta oxide minerals (Fig. 5). Composition of zircon strongly depends on the fractionation degree of parental granitic rock: concentrations of Hf and Sc generally increase from less fractionated biotite granites to the most fractionated topaz-zinnwaldite granite and quartz albitite or from core to rim (Table 5).

The HfO_2 content and Zr/Hf wt. ratio attain 1.4–4.1 wt. % and 38–13 in biotite granites, 2.0–2.6 wt. % and 30–20 in tourmaline granite, 3.3–13 wt. % and 14.5–3.5 in topaz granite, and 6.6–12 wt. % and 7.9–4.0 in albitite, respectively (Fig. 6a).

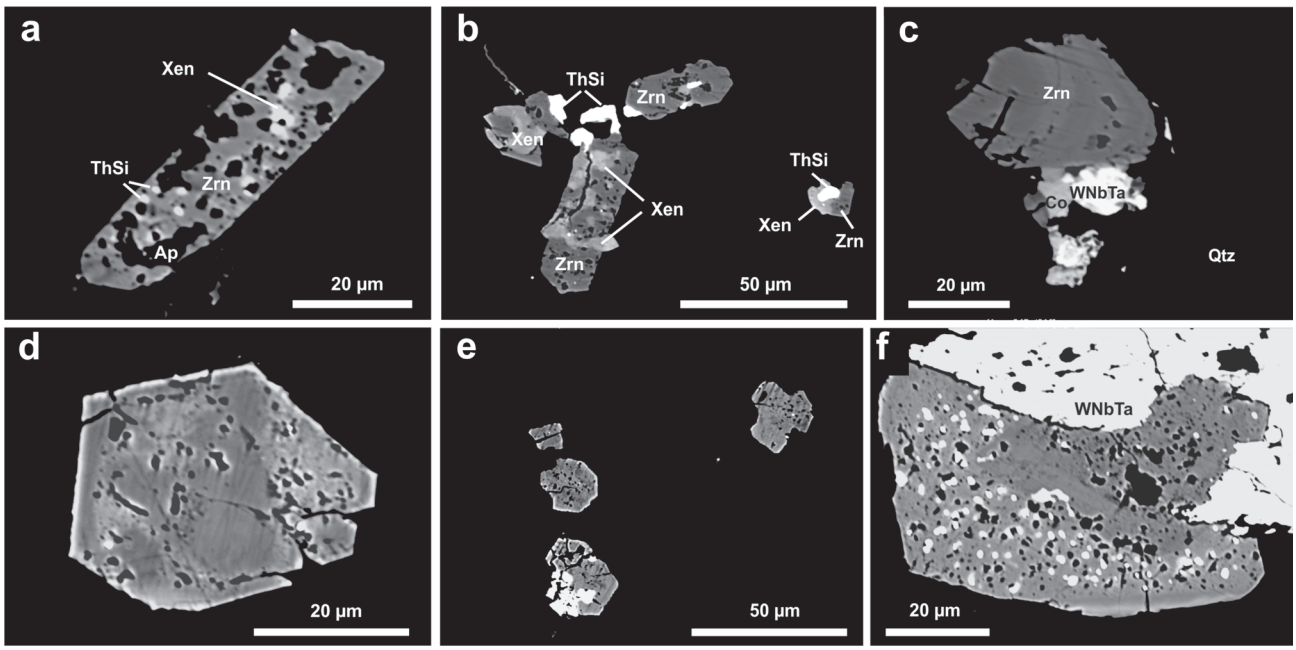

Fig. 5. BSE photomicrographs of zircon from the Dlhá dolina granites. **a** — Elongated zircon crystal with inclusions of fluorapatite (anhedral black), xenotime (larger white) and thorite/huttonite (smaller white), biotite granite (sample 3641); **b** — Zircon crystals (dark grey) with xenotime intergrowths (pale grey) and thorite/huttonite (white), tourmaline granite (sample 3638); **c** — Zircon crystal (dark grey) with ferrocolumbite (pale grey) and W-rich ixiolite/columbite phase (white), tourmaline granite (sample 3638); **d** — Euhedral zircon crystal with diffuse zoning, mylonitized topaz granite (sample 3634); **e** — Zircon crystals and intergrowths of uraninite + ferrocolumbite + microlite phase (white) in muscovite, mylonitized topaz granite (sample 3634); **f** — Zircon (grey) with numerous tiny inclusions of uraninite, rarely cassiterite (white) in association with W-rich ixiolite/columbite phase (large white mineral, upper part of figure), topaz granite (sample 3633).

Table 4: Representative compositions (in wt. %) and empirical formulae (based on 22 oxygen atoms) of micas. Contents of Li_2O were calculated only in primary magmatic Mg-free micas according to algorithms by Breiter et al. (2002).

Sample	3626	3628	3629	3631	3633	3633	3638	3640	3641
Rock	Albitite	Silicified albitite	Mylonitized albitite	Mylonitized topaz granite	Topaz granite	Topaz granite	Tourmaline granite	Biotite granite	Biotite granite
Proposed name of mica	Fengite	Fengite	Flogopite	Fengite	Zinnwaldite	Zinnwaldite	Fengite	Fengite	Fengite
SiO_2	47.95	48.99	40.83	47.27	49.08	48.57	47.76	48.18	47.88
TiO_2	0.08	0.04	0.35	0.00	0.14	0.22	0.16	0.06	0.36
Al_2O_3	32.99	30.12	13.24	32.29	19.44	19.45	31.31	27.65	28.85
FeO	0.43	1.39	9.35	0.49	9.38	8.70	4.45	5.92	6.10
MgO	1.35	2.04	20.06	1.91	0.05	0.04	0.45	1.34	1.50
MnO	0.01	0.01	0.00	0.05	0.38	0.52	0.15	0.25	0.22
CaO	0.00	0.00	0.01	0.00	0.00	0.00	0.00	0.00	0.00
BaO	0.05	0.01	0.00	0.00	0.00	0.00	0.00	0.00	0.00
Na_2O	0.59	0.27	0.10	0.91	0.07	0.07	0.23	0.11	0.10
K_2O	10.94	11.51	9.98	10.15	10.63	10.42	10.83	11.19	10.74
Rb_2O	0.05	0.13	0.45	0.11	1.11	1.49	0.08	0.12	0.14
Li_2O calc					3.94	3.77			
F	0.60	1.23	3.04	0.42	7.69	7.57	1.27	0.00	0.00
F=O	–0.23	–0.47	–1.15	–0.16	–2.90	–2.86	–0.48	0.00	0.00
Total	94.81	95.27	96.25	93.44	99.02	97.97	96.19	94.82	95.89
Si	6.421	6.606	5.991	6.407	6.918	6.921	6.455	6.634	6.510
Al	1.579	1.394	2.009	1.593	1.082	1.079	1.545	1.366	1.490
X	1.000	1.000	1.000	1.000	1.000	1.000	1.000	1.000	1.000
Ti	0.008	0.004	0.039	0.000	0.015	0.024	0.016	0.007	0.037
Al	3.627	3.393	0.282	3.565	2.147	2.188	3.442	3.121	3.132
Fe	0.048	0.157	1.147	0.056	1.106	1.037	0.503	0.682	0.693
Mg	0.269	0.410	4.388	0.386	0.011	0.009	0.090	0.274	0.304
Mn	0.001	0.001	0.000	0.006	0.046	0.062	0.017	0.029	0.025
Ca	0.000	0.000	0.001	0.000	0.000	0.000	0.000	0.000	0.000
Ba	0.003	0.000	0.000	0.000	0.000	0.000	0.000	0.000	0.000
Li					2.226	2.152			
Y	3.955	3.966	5.856	4.013	5.550	5.472	4.068	4.113	4.191
Na	0.154	0.069	0.028	0.238	0.019	0.020	0.061	0.030	0.027
K	1.869	1.980	1.867	1.755	1.912	1.894	1.867	1.965	1.862
Rb	0.005	0.011	0.043	0.010	0.100	0.137	0.007	0.010	0.012
Z	2.028	2.061	1.938	2.003	2.031	2.051	1.935	2.005	1.901
F	0.253	0.526	1.411	0.178	3.426	3.413	0.542	0.000	0.000
Mg/(Mg+Fe)	0.85	0.72	0.79	0.87	0.01	0.01	0.15	0.29	0.30

Table 5: Representative compositions of zircon (in wt. %, contents of La, Pr, Nd, Sm, Eu, Tb, Ho, Tm, Lu, and Mn are under detection limit of EMPA).

Rock	Biotite granite	Biotite granite	Tourm. granite	Tourm. granite	Topaz granite	Topaz granite	Topaz granite	Topaz granite	Quartz albitite	Quartz albitite
Sample No.	3641/4	3641/5	3638/1	3638/2	3633/2	3633/3	3633/6	3633/7	3629/1	3629/2
Crystal/Position	2/center	2/rim	1/center	1/rim	2/center	2/rim	3/rim	4/center	1/center	1/rim
P_2O_5	0.75	0.59	0.83	0.95	2.00	**3.49**	**2.91**	1.94	0.09	0.21
As_2O_5	0.13	0.17	0.14	0.16	0.19	0.25	**0.49**	0.22	**0.40**	**0.44**
Nb_2O_5	0.00	0.00	0.00	0.00	0.24	0.18	0.19	0.21	0.00	0.00
SiO_2	32.40	32.26	32.27	31.76	30.26	28.87	28.91	30.39	31.50	31.59
ZrO_2	63.23	62.76	61.63	60.91	59.54	54.80	49.28	56.78	53.35	53.25
HfO_2	2.21	3.15	1.98	2.30	4.10	3.76	**11.99**	3.67	**11.75**	**11.71**
ThO_2	<0.03	<0.03	0.07	0.03	0.03	0.04	<0.03	0.05	<0.03	0.08
UO_2	0.82	0.73	0.51	1.11	1.29	2.70	3.25	2.32	0.61	1.30
Al_2O_3	<0.03	0.03	<0.03	0.05	0.13	0.25	0.24	0.21	<0.03	<0.03
Sc_2O_3	0.16	0.20	0.20	0.30	1.16	**1.94**	**2.15**	1.14	0.27	0.35
Y_2O_3	0.47	0.47	0.74	0.73	0.55	0.90	0.03	0.62	<0.03	<0.03
Ce_2O_3	0.05	0.05	0.03	0.04	0.07	0.04	0.03	<0.03	<0.03	0.05
Gd_2O_3	0.00	0.05	<0.03	0.06	<0.03	<0.03	<0.03	<0.03	0.10	0.12
Dy_2O_3	0.08	0.08	<0.03	0.04	<0.03	<0.03	<0.03	<0.03	0.04	0.03
Er_2O_3	0.37	0.37	0.42	0.37	0.39	0.39	0.43	0.38	0.22	0.26
Yb_2O_3	0.29	0.26	0.37	0.30	0.23	0.37	0.18	0.28	0.10	0.11
Fe_2O_3	0.08	0.10	0.11	0.16	0.08	0.14	0.21	0.63	0.11	0.14
CaO	0.09	0.04	0.05	0.04	0.15	0.36	0.27	0.27	<0.03	<0.03
SrO	<0.03	<0.03	<0.03	<0.03	0.08	0.08	0.08	0.10	0.05	0.05
Total	101.13	101.31	99.35	99.31	100.49	98.56	100.64	99.21	98.59	99.69
P	0.019	0.015	0.022	0.025	0.052	0.093	0.079	0.051	0.002	0.006
As	0.002	0.003	0.002	0.003	0.003	0.004	0.008	0.004	0.007	0.007
Nb	0.000	0.000	0.000	0.000	0.003	0.003	0.003	0.003	0.000	0.000
Si	0.989	0.988	0.998	0.988	0.938	0.908	0.923	0.952	1.021	1.016
Al	0.000	0.001	0.000	0.002	0.005	0.009	0.009	0.008	0.000	0.000
Sum *B*	1.010	1.007	1.022	1.018	1.001	1.017	1.022	1.018	1.030	1.029
Zr	0.942	0.938	0.929	0.924	0.900	0.841	0.767	0.868	0.843	0.835
Hf	0.019	0.028	0.017	0.020	0.036	0.034	0.109	0.033	0.109	0.108
Th	0.000	0.000	0.000	0.000	0.000	0.000	0.000	0.000	0.000	0.001
U	0.006	0.005	0.004	0.008	0.009	0.019	0.023	0.016	0.004	0.009
Sc	0.004	0.005	0.005	0.008	0.031	0.053	0.060	0.031	0.008	0.010
Y	0.008	0.008	0.012	0.012	0.009	0.015	0.001	0.010	0.000	0.000
Ce	0.001	0.001	0.000	0.000	0.001	0.000	0.000	0.000	0.000	0.001
Gd	0.000	0.001	0.000	0.001	0.000	0.000	0.000	0.000	0.001	0.001
Dy	0.001	0.001	0.000	0.000	0.000	0.000	0.000	0.000	0.000	0.000
Er	0.004	0.004	0.004	0.004	0.004	0.004	0.004	0.004	0.002	0.003
Yb	0.003	0.002	0.003	0.003	0.002	0.004	0.002	0.003	0.001	0.001
Fe	0.002	0.002	0.003	0.004	0.002	0.003	0.005	0.015	0.003	0.003
Ca	0.003	0.001	0.002	0.001	0.005	0.012	0.009	0.009	0.000	0.000
Sr	0.000	0.000	0.000	0.000	0.001	0.001	0.001	0.002	0.001	0.001
Sum *A*	0.993	0.996	0.979	0.985	1.000	0.986	0.981	0.991	0.972	0.973
Sum cat.	2.003	2.003	2.001	2.003	2.001	2.003	2.003	2.009	2.002	2.002
Zr/Hf wt.	24.98	17.39	27.17	23.12	12.68	12.72	3.59	13.51	3.96	3.97
$HREE_2O_3$	0.74	0.76	0.79	0.77	0.62	0.76	0.61	0.66	0.46	0.52
HREE apfu	0.008	0.008	0.007	0.008	0.006	0.008	0.006	0.007	0.004	0.005

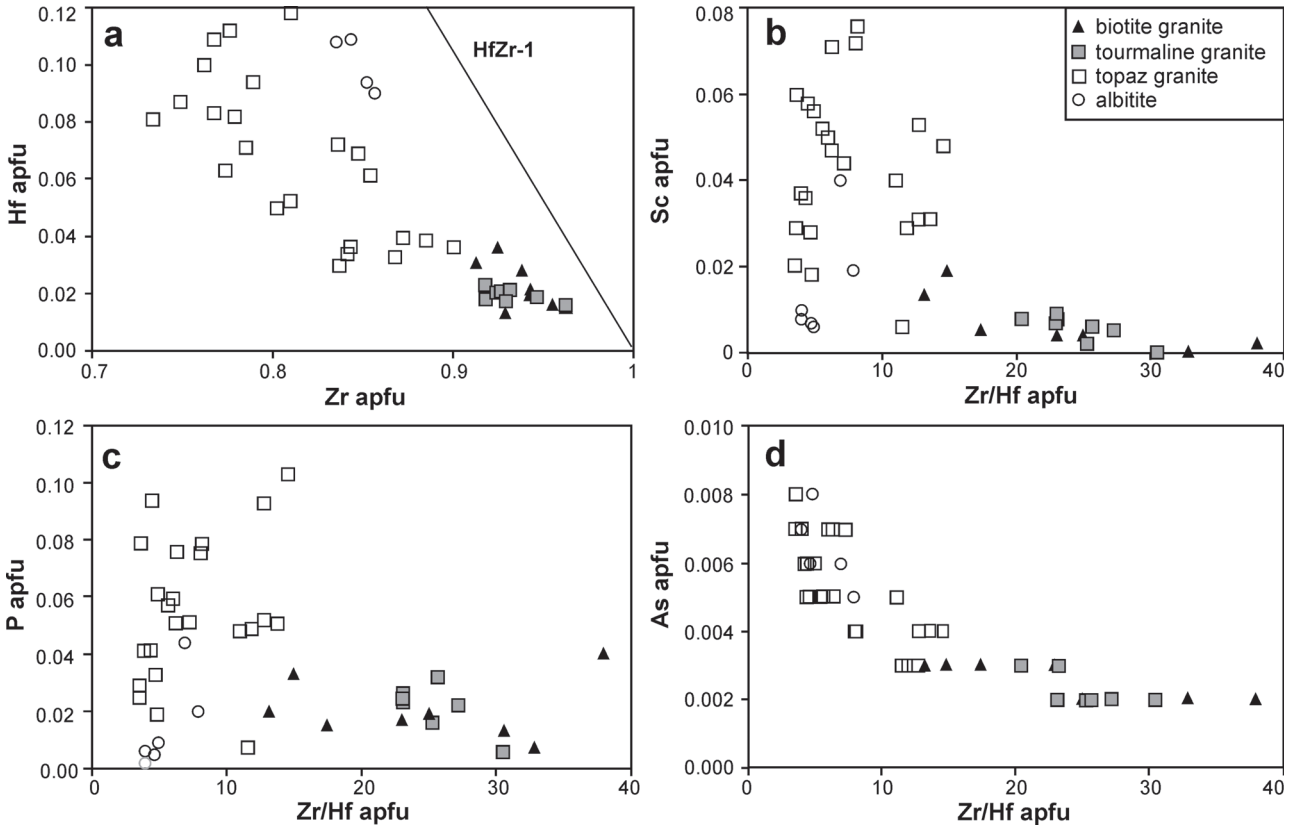

Fig. 6. Chemical composition of zircon from Dlhá dolina granites in atoms per formula unit. **a** — Zr vs. Hf, **b** — Zr/Hf vs. Sc, **c** — Zr/Hf vs. P, **d** — Zr/Hf vs. As.

In both suites contents of Sc increased upwards, while contents of Y decreased: from 0.0–0.2 to 0.1–0.7 wt. % Sc_2O_3 and 0.2–1.6 to 0.2–0.5 wt. % Y_2O_3 in biotite granites, and from 0.1–0.3 to 0.8–2.8 wt. % Sc_2O_3 (Fig. 6b) and 0.5–1.0 to 0.0-0.6 wt. % Y_2O_3 in Li-mica granites. However, zircon from the topaz granite occasionally shows irregular Y, HREE-rich zones with 1 to 2 wt. % Y_2O_3. Contents of REEs in zircon are generally low to moderate, heavy REE (HREE — Gd to Lu) apparently prevail over light REE (LREE — La to Eu), attaining 0.3 to 1 wt. % $HREE_2O_3$ in all studied granite types.

The contents of phosphorus attain 0.1 to 3.8 wt. % P_2O_5 (up to 0.1 apfu P, Fig. 6c), it positively correlates with trivalent A-site cations, especially Sc and Y. Moreover, zircon from the most evolved granites reveals elevated niobium concentrations: up to 0.4 wt. % Nb_2O_5 in albitite and up to 0.9 wt. % Nb_2O_5 (0.013 apfu Nb) in topaz granite. Slightly elevated contents of Al (up to 0.25 wt. % Al_2O_3; 0.01 apfu Al), Fe (max. 0.6 wt. % Fe_2O_3; 0.015 apfu Fe), Ca (up to 1.0 wt. % CaO; 0.03 apfu Ca) and Sr (max. 0.1 wt. % SrO; 0.002 apfu Sr) are characteristic mainly for the (metamictized?) zircons from the topaz granite. Elevated contents of As (up to 0.5 wt. % As_2O_3; 0.008 apfu As, Fig. 6d) in some zircons from topaz granite and albitite may indicate reequilibration with hydrothermal fluid during greisenization.

The compositional relationships indicate a presence of $HfZr_{-1}$, $ScP(Zr,Hf)_{-1}Si_{-1}$, $YP(Zr,Hf)_{-1}Si_{-1}$, and especially $(Sc,Y)(P, As,Nb)(Zr,Hf)_{-1}Si_{-1}$ substitutions in the majority of analysed zircon crystals. However, limited $AlPSi_{-2}$, berlinite-type substitution could also play a role. Uranium-rich compositions commonly show positive correlation with Fe and Ca.

Fluorapatite

Fluorapatite in the biotite granites should be considered as a magmatic mineral. It forms homogeneous, mostly isometric grains, 20–50 μm across. Fluorapatite is sometimes included in mica; in other cases it is interstitial. It is fully saturated in fluorine and relatively poor in Mn (0.1–1.4 wt. % MnO, up to 0.1 apfu Mn), but slightly enriched in Ce (max. 0.3 wt. % Ce_2O_3).

Fluorapatite within the Li-mica granites and albitite was strongly affected by the Alpine low-temperature processes. Individual crystals or their parts differ greatly in intensity and colour of CL: from intensive yellow through red and violet to yellowish-grey. The intensity of CL generally increases with increasing contents of Mn, Fe, and Sr, but without clear correlation to one of the above mentioned elements. The distribution of Mn, Fe, and Sr is highly variable not only between samples, but also within individual grains (Table 6). Maximum contents of minor elements in fluorapatite from Li-mica granites attain 3.0 wt. % MnO (0.22 apfu Mn), 0.6 wt. % FeO (0.05 Fe), and 1.8 wt. % SrO (0.09 apfu Sr).

Within albitite, including their silicified (greisenized) parts, fluorapatite variegated in even broader intervals as in the granites: 0–3.3 wt. % MnO (0.25 apfu Mn), 0–0.6 wt. % FeO

Table 6: Representative composition (in wt. %) and empirical formulae (based on 12.5 oxygen atoms) of fluorapatite (contents of Ti, Al, Mg, Ba, Rb, Ce, and Cl are under the detection limit of the microprobe). Content of F fitted to the maximum amount of (F + Cl + OH) = 1 when overestimated by analysis.

Sample	3628	3628	3628	3641	3631
Rock	Albitite	Albitite	Albitite	Topaz granite	Biotite granite
Colour in CL	violet	red	yellow	yellow	yellow
SiO_2	0.00	0.00	0.00	0.06	0.00
FeO	0.00	0.00	0.62	0.28	0.00
MnO	0.00	0.00	2.77	1.42	0.60
CaO	55.85	55.83	48.50	53.75	54.05
SrO	0.00	0.00	5.67	0.00	1.85
Na_2O	0.00	0.00	0.08	0.13	0.05
K_2O	0.00	0.00	0.00	0.13	0.00
P_2O_5	42.82	42.51	41.20	41.94	42.08
F	3.61	3.75	3.66	3.75	3.75
F=O	–1.52	–1.62	–1.55	–1.56	–1.56
Total	100.75	100.56	100.89	99.87	100.81
Si	0.001	0.001	0.001	0.005	0.000
Fe	0.000	0.001	0.046	0.019	0.002
Mn	0.002	0.000	0.206	0.102	0.043
Ca	4.968	4.990	4.570	4.855	4.906
Sr	0.000	0.000	0.289	0.000	0.091
Na	0.000	0.000	0.013	0.021	0.008
K	0.000	0.000	0.000	0.014	0.000
P	3.010	3.002	3.067	2.993	3.018
F	0.947	0.989	1.000	1.000	1.000

Table 8: Representative compositions (in wt. %) and empirical formulae (based on 24 oxygen atoms) of tourmaline (contents of Ba, Rb, P, and F are under the detection limit of EMPA).

Rock	Tourmaline granite	Tourmaline granite	Biotite granite	Biotite granite
Sample	3638	3638	3641	3641
Colour	brown	brown	blue	blue
SiO_2	33.94	35.99	35.89	36.18
TiO_2	0.90	0.26	0.12	0.02
Al_2O_3	28.87	29.83	30.42	34.41
FeO	18.68	12.12	14.91	13.63
MgO	0.58	4.53	3.06	1.63
MnO	0.24	0.11	0.19	0.14
CaO	0.02	0.03	0.60	0.15
Na_2O	2.80	2.81	2.50	1.97
K_2O	0.07	0.07	0.06	0.05
F	<0.05	0.17	<0.05	0.00
F=O		–0.06		
Total	86.20	85.86	87.76	88.18
Si	5.941	6.086	6.021	5.939
Ti	0.119	0.033	0.016	0.002
Al	5.955	5.944	6.015	6.657
Fe	2.734	1.713	2.091	1.871
Mg	0.151	1.141	0.765	0.398
Mn	0.035	0.016	0.028	0.020
Ca	0.003	0.005	0.108	0.027
Na	0.951	0.922	0.814	0.626
K	0.016	0.016	0.012	0.011
F	0.000	0.089	0.000	0.000

(0.05 Fe), and up to 7.5 wt. % SrO (0.39 apfu Sr). As in Li-mica granites, all fluorapatites are F-saturated and free of Cl and Ce.

Tiny fluorapatite grains disseminated in feldspars or filling small cracks in older minerals show conspicuous bright yellow colour in CL, but they are too small to be analyzed.

Table 7: Representative composition (in wt. %) and empirical formulae (based on 5 oxygen atoms) of topaz from the sample 3633. Contents of elements Ti, Mg, Ca, Ba, Rb, Na, and K in all cases lower than detection limit 0.05 wt. %.

SiO_2	32.37	32.58	32.33	32.39	32.56
Al_2O_3	56.09	55.72	55.68	55.42	55.67
FeO	0.00	0.00	0.00	0.06	0.04
MnO	0.00	0.00	0.07	0.00	0.08
P_2O_5	0.00	0.08	0.21	0.19	0.08
F	20.72	20.80	20.76	21.39	20.84
F=O	–8.76	–8.80	–8.78	–9.05	–8.81
Total	100.42	100.39	100.27	100.41	100.45
Si	0.987	0.994	0.988	0.992	0.994
Al	2.016	2.004	2.005	2.000	2.002
Fe	0.000	0.000	0.000	0.002	0.001
Mn	0.000	0.001	0.002	0.000	0.002
P	0.000	0.002	0.005	0.005	0.002
F	1.998	2.007	2.006	2.072	2.011

Topaz

Euhedral, probably late-magmatic interstitial crystals of topaz, up to 1 mm in size, were encountered only in the topaz granite. The crystals show fine oscillatory zoning and tiny cracks filled by secondary fluorapatite. Topaz is fully saturated in fluorine (~2.0 apfu F) and slightly enriched in phosphorus (up to 0.2 wt. % P_2O_5; ≤0.005 apfu P, Table 7).

Tourmaline

Fine grains of tourmaline (max. 0.1 mm across), bluish in polarized light, scarcely occur in the biotite and tourmaline granites. Macroscopically black tourmaline, brownish in polarized light, is common in the lower part of the younger intrusive suite. It is disseminated as small individual grains or forms aggregates up to several cm across. According to its chemical composition, both varieties of tourmaline should be termed as schorlitic tourmaline with Fe/(Fe + Mg) ratio between 0.60 to 0.95 and a low concentration of F (up to 0.2 wt. %) (Table 8).

Discussion

Evolution of micas in the Dlhá dolina pluton

To distinguish the primary high-temperature (Variscan) and low-temperature (Alpine) micas and to assess the degree of secondary overprint of the former, we examined several diagrams (Fig. 4a,b). Already published analyses of micas from the Surovec granite and the Dlhá dolina topaz granite (Petrík et al. 2011, 2014) and representative analyses of pure magmatic micas from the peraluminous P-F-Li rich granitic system of Nejdek-Podlesí, western Krušné hory Mts (Breiter 2002; Breiter et al. 2005) are plotted in all diagrams for comparison. All micas from the DD-3 borehole are rich in alumina containing 4.8–5.3 apfu Al (Table 4). The content of Al in the octahedral position usually reached 3.3–3.5 apfu, which indicated that most of the analysed micas are di-octahedral. The exceptions are altered biotite from the biotite granites (Al^{VI}~3)

and zinnwaldite from the "fresh" topaz granite at the depth of 580 m (Al^{VI}~2.7–2.9). The low total of divalent elements (Fe + Mg + Mn < 1 apfu, Fig. 4a) and especially the low content of Fe (mostly < 1 apfu) is a logical counterpart of the high Al^{VI}. The unusually high content of MgO and thus high #Mg (atomic ratio Mg/(Mg + Fe)) of the majority of micas from the Dlhá dolina pluton is noticeable at the first view. With the exception of the relatively less tectonically affected sample of the topaz-zinnwaldite granite (MgO < 0.1 wt. %, #Mg < 0.05), the MgO and #Mg are substantially higher than usual in micas from fractionated granites or leucogranites (Fig. 4b, compare the compilation in Tischendorf et al. 1999).

Fig. 4b summarizes the changes in chemical composition from slightly Fe-deficient, but still F, Li-rich zinnwaldite from the topaz granite at a depth of 580 m, the Alpine Li-rich phengite (altered primary Li-Fe mica) from the tourmaline granite, to Mg-enriched F-free phengite from the uppermost strongly mylonitized part of the topaz granite and albitite.

Published data from the Dlhá dolina granites (Petrík et al. 2014) are closer to the theoretical magmatic evolution than our data, because they analysed the tectonically least affected parts of the borehole DD-3, while we studied samples from the whole core to ascertain the extent of post-magmatic changes. Summarizing all the available data, following scenario of mica evolution can be proposed:

- The deeper suite of biotite granites: primary annite was partially chloritized and/or muscovitized. Timing of the alteration (post-magmatic vs. Alpine) is not clear;
- The upper suite, tourmaline granite: primary Li-mica (protolithionite?) was partially muscovitized (Li, Fe, F-decreased), but not enriched in Mg;
- The upper suite, topaz granite: primary zinnwaldite is preserved in tectonically undeformed domains. In deformed parts, the mica was muscovitized (Li, F, Fe-decreased) producing Li-rich phengite from the surface of mineral grains downwards, and enriched in Mg;
- The upper suite, albitite: all textural types of mica represent Mg-rich muscovite (phengite), as a result of the Alpine overprint. The primary character of these micas cannot be deciphered, but part of the micas with relatively higher fluorine (0.5–1.5 apfu F) could by remnants after primary zinnwaldite. The F-poor micas represent the low-temperature Alpine generation.

Magmatic evolution of the Dlhá dolina pluton

Abrupt changes in contents of some chemical elements support sharp, intrusive contact between the lower barren and the upper rare-metal granite suites in the Dlhá dolina pluton. Moreover, these granites were tectonically modified (Fig. 2). Both granite suites represent late-orogenic peraluminous crustal melts. While the deeper intrusion formed a chemically homogeneous body, the upper magma batch underwent differentiation in situ resulting in remarkable stratification.

The direction and manner of crystallization of the upper suite resulted mainly from a combination of two factors: chemical stratification within the water- and fluxes-rich magma batch (London 2014), and cooling. Petrasová et al. (2007) estimated the metamorphic conditions in the country rock during the intrusion of Li-mica granites near 100 MPa and 430 °C. This means relatively shallow, nearly sub-volcanic conditions with a fast cooling rate of the granites.

The increase of Na, F, P, Li, and Rb combined with decrease of Si, K, Fe in the depth interval from 720 to 550 m upwards (Fig. 7a) are mineralogically expressed in transition of the tourmaline (+Li-rich biotite or protolithionite) to the topaz (+zinnwaldite) granite. The uppermost part of the topaz granite (in the depth of 575–550 m) is strongly affected by shearing and primary character of the contact between topaz granite and overlaying albitite is difficult to interpret. Presence of some K-feldspar in approximately the lowermost 50 m of the albitites (in the depth of 550–500 m) suggests that the contact between topaz granite and quartz albitite was primarily transitional. This transition is marked by increases of Na, Ga, Nb, Ta, and Sn and decreases of K, Fe, P, F, Li, Rb, Cs, W, Y, and REE. Contents of Si, Al, and Zr remain the same.

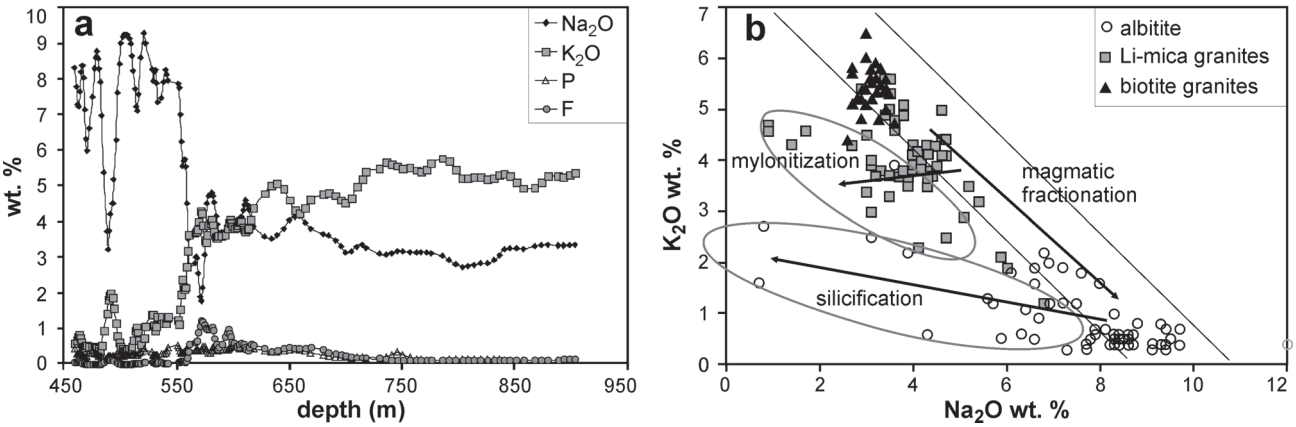

Fig. 7. Distribution of some chemical elements in the borehole DD-3, the Dlhá dolina pluton. **a** — Contents of Na_2O, K_2O, P, and F along the borehole DD-3 (moving average of 5 adjacent samples, computed by authors from original data of Malachovský et al. 1992); **b** — Correlation between Na_2O and K_2O in rocks from the borehole DD-3 (data from Malachovský et al. 1992). The sum of the alkali oxides in magmatic rocks ranges between 8–10 wt. %; during fractionation contents of Na_2O generally increased, while K_2O decreased. Decrease in Na_2O in some samples is caused by mylonitization (in Li-mica granites) and silicification-greisenization (in albitite).

The sum of the alkalis (Na_2O+K_2O) in all the rock facies varies in a relatively narrow interval 8–10 wt. % (Fig. 7b) and is consistent with fully magmatic origin of the albitite. Albite grains in the albitite are enriched in phosphorus suggesting their primary magmatic origin (London et al. 1993; Breiter et al. 2002). Also the texture of non-mylonitized albitite is consistent with crystallization from melt; no signs of Na-metasomatosis were found. Thus, the upper part of the magma batch should have been enriched in Na before the feldspar started to crystallize. We found no indications of later additional metasomatic input of alkalis into the albitite. Differentiation of crystallized hydrous silicate melt into K- and Na-dominated domains is typical for layered aplite-pegmatite systems (Jahns 1955; London 2014). Among lithophile elements, if we neglect the irregularities caused by the low-temperature Alpine overprint, the primary magmatic contents of Li, Rb, Sn, Nb, and Ta in tourmaline and topaz granites increased systematically upwards: ca. 400→1200 ppm Rb, 200→1000 ppm Li, 50→250 ppm Sn, 2060 ppm Nb, and 10→100 ppm Ta. Sharp decreases of Rb- and Li-contents in the albitite are caused by nearly complete disappearance of Li-mica and an abrupt decrease of K-feldspar. The systematic increase of Sn, Nb and Ta in the upper part of the cupola does not correlate with the extent of greisenization and suggests a mostly magmatic origin of disseminated columbite in albitite. Distribution of Sn is much more scattered, but the highest contents of Sn were encountered in the Na-most enriched domains of the albitite body (Fig. 8). In contrast, the highest contents of W were found in the topaz granite. Decoupling of Nb+Ta and Sn and W during final stage of fractionation of peraluminous F, Li-rich granite was also described from the Podlesí granite stock, Krušné hory Mts, Czech Republic (Breiter et al. 2007).

The absence of signs of greisenization within the topaz and tourmaline granite made any later supply of fluids (+ore elements) from the depth unlikely. Separation of greisenizing fluids from the melt should appear *in situ* already during crystallization of the tourmaline and mainly topaz granite. The irregular, but dominantly steep joins may have formed via hydrofracturing during "second boiling" of the residual melt.

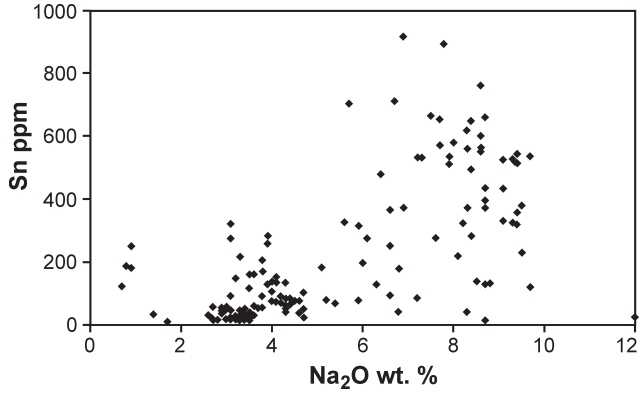

Fig. 8. Contents of Na and Sn in 1–2 m long segments of the borehole DD-3, the Dlhá dolina pluton (primary data from Malachovský et al. 1992). Enrichment of tin correlated well with high content of albite. The "greisenized" samples poor in Na are relatively Sn-poor.

Low degree of greisenization

According to the original description by Malachovský et al. (1992) greisenization (early post-magmatic silicification) along sub-vertical (?)cm-dm-scale joins affected only the albitite.

Among 65 samples of 1–2 m long segments of the core from the albitite (depth 454–554 m, Malachovský et al. 1992), only two samples from the depth 488 and 489.5 m contain less than 1 wt. % of Na_2O and should be designated as greisen. Moreover, 7 samples contain 3.5–5.9 wt. % Na_2O, and another 56 samples contain more than 6.0 wt. % Na_2O. Thus, excluding the section 486–489 m, the range of silicification (greisenization) of the albitite is minimal. Above that, the Si-rich samples are Li-poor (<100 ppm Li) and Sn does not correlate positively with Si, but with Na. The "greisens" are slightly enriched in apatite; necessary phosphorus was liberated from crystal lattice of altered albite. Summing up, the range of greisenization in the DD-3 section and its influence on mineralization is minimal, if it occurs at all.

Low-temperature Alpine overprint

The conditions of the Alpine metamorphism in the Dlhá dolina area were estimated at 350 °C and 180–280 MPa (Radvanec et al. 2004), however distinctly higher pressures (~400 °C and 600–700 MPa) were reported by Petrasová et al. (2007). The granite body was affected by shearing and mylonitization. The intensity of mechanical deformation is highly variable: zones composed of only relicts of magmatic quartz flowing in aggregates of fine-grained phengitic muscovite alternate with nearly fresh primary granite and albitite. The brittle deformation of granitoids was accompanied by supply of fluids from dolomite, magnesite and talc bodies to the granite cupola (Kilík 1997; Radvanec et al. 2004; Petrasová et al. 2007). These fluids, enriched in Ca, Mg and CO_2, permeated the upper part of the granite body resulting in crystallization of Ca, Mg-carbonates in thin joints and small cavities. Carbonate minerals, inconspicuous under an optical microscope, are clearly detectable on CL-images. During this process, the whole-rock content of Mg was enriched up to 0.9 wt. % in mylonitized albitite and up to 1.7 wt. % in mylonitized topaz granite. Similarly, Ca was enriched up to 1.4 and 2.9 wt. % in albite and granite, respectively. Exhumation (end of the metasomatic processes) was dated to 87.7 (±5.9 Ma) using zircon fission-track analyses (Plašienka et al. 2007).

Comparison of the Dlhá dolina pluton with other Gemeric granites

Three other granite bodies cropped out in the vicinity of the Dlhá dolina pluton. The geographically closest body, the Surovec granite, is also the most similar from the point of view of chemical composition (enrichment in F, P, and Li), mineralogy (topaz, zinnwaldite, P-rich primary feldspars), and strong Alpine overprint. The bodies near Hnilec and Betliar are B-specialized containing common tourmaline in association with Li-poor micas.

The mineral composition of the Surovec body published by Petrík et al. (2011, 2014) allows a comparison with the Li-granites from the Dlhá dolina granite system, whereas analogues of albitite and biotite granite were not found in the Surovec body. In both localities, remnants of primary magmatic mineral assemblages alternate with domains of strong Alpine low-temperature hydrothermal overprint. Increasing intensity of the overprint is marked by nearly complete loss of phosphorus in feldspars (from 1.5 to <0.1 wt. % P_2O_5 in Surovec, from 0.5 to <0.1 wt. % P_2O_5 in Dlhá dolina) and transformation of primary zinnwaldite (5–11.5 wt. % FeO in Surovec, 8.7–9.4 wt. % FeO in Dlhá dolina) to secondary Li-rich phengite (5–7.5 wt. % FeO in Surovec, 0.4–4.5 wt. % FeO in Dlhá dolina). Fluorapatite, which was primarily Mn-rich (up to 6 wt. % MnO in Surovec and 3.3 wt. % MnO Dlhá dolina) was metasomatically strongly enriched in Sr (up to 13.6 wt. % in Surovec and 5.7 wt. % SrO in Dlhá dolina). A specific feature of the Dlhá dolina granites is the enrichment of secondary micas in magnesium (commonly ~2 wt. % in phengitic muscovite and up to 20 wt. % in flogopite), which may be attributed to the processes of steatization of the nearby Gemerská Poloma talc deposit (Kilík 1997; Radvanec et al. 2004). Topaz from both localities differs significantly: while topaz from Surovec granite is enriched in phosphorus (up to 1.2 wt. % F) and relatively poor in F (14–15 wt. %, only 68–75 atom. % of (F+OH)-site occupancy); topaz from Dlhá dolina is P-poor (max. 0.2 wt. % P_2O_5), but F-rich (20–21 wt. % F, ~100 atom. % of (F+OH)-site occupancy). The composition of the Dlhá dolina topaz fits well with topaz from peraluminous topaz-zinnwaldite granites in the western Erzgebirge (Breiter & Kronz 2004), while the Surovec topaz was probably re-equilibrated during Alpine processes. The differences in composition of topaz, apatite and secondary micas, and the appearance of varied assemblages of hydrated secondary phosphate minerals (Petrík et al. 2011) indicate somewhat different *P-T* conditions and composition of Alpine hydrothermal fluids at the two localities.

We interpret the Dlhá dolina pluton as a combination of two intrusive pulses: (i) biotite granites, and (ii) Li-mica granites + albitite. Two-stage granite evolution has also been reported from the nearby Betliar and Hnilec areas. However, in Betliar, the first magmatic stage has formed evolved volatile rich magmas which intruded into an open fault system as sill-like bodies crystallizing as equigranular fine-grained granites followed by subsequent high-temperature post-magmatic alteration. The second stage intrusion from a deeper seated magmatic reservoir resulted in formation of the porphyric granite body. The emplacement of both granite intrusions were dated as Middle or Late Permian (Kubiš & Broska 2010).

In the Hnilec area, volatiles (mainly B, in a lesser amount also F) concentrated in hydromagma under the carapace of fast quenched fine-grained granites. Overpressure due to separation of B-rich fluids caused hydrofracturing of roof fine-grained granites and exocontact rocks. The F-rich portion of the fluid greisenized some domains in the endocontact. The porphyric to coarse-grained two-mica and biotite granites are situated below this fine-grained metasomatized and greisenized granite carapace (Kubiš & Broska 2005).

Comparison with other rare-metal granites worldwide

Two main genetically important issues should be discussed to correctly interpret the geological structure and development of the Dlhá dolina pluton: (i) time/space relation of the less- and more evolved rock types (biotite granites *vs.* Li-mica granites), and (ii) relations between the most-evolved ore-bearing granite facies, feldspatite and greisens.

The simplified vertical cross-section of the Dlhá dolina is compared with several long time studied and thus well recognized Sn, W, Nb, Ta-bearing plutons from the Krušné hory/Erzgebirge and French Massif Central (Fig. 9). Among the five compared profiles, only the Sn, W-mineralized Krásno pluton (Jarchovský 1998, 2004) is composed of one intrusion. In all other plutons, two intrusive units were recognized and the more-evolved rock suites are situated in the upper part of the profiles above the less-fractionated granites. Both suites have sharp intrusive contacts, but they are interpreted as co-magmatic. In Cínovec and Podlesí (both the Krušné hory, Czech Republic), the younger Li-mica granite formed a tongue-like body which intruded generally along the contact plane between the older biotite granite and its envelope (Štemprok et al. 1994; Breiter et al. 2005). The origin of the Beauvoir pluton (France) was interpreted in another way: the more-evolved part of the melt, due to lower viscosity, intruded faster and crystallized in the upper part of the cupola. The less evolved more viscose part of the melt arrived later and remained in the lower part of the known profile (Raimbault et al. 1995). In the Dlhá dolina, the relative age relation between the lower and upper granite suites remains unresolved.

Comparing the Dlhá dolina magmatic system with well-known Sn-W greisen deposits in the Krušné hory/Erzgebirge, such as Geyer and Ehrenfriedersdorf (Hösel 1994) in (Germany), and Krásno (Jarchovský 2004) and Cínovec (Štemprok & Šulcek 1969), both Czech Republic, the major difference should be seen in the position of feldspar-rich rocks (feldspatites, albitites) in the vertical evolution of the granite cupola, and time/space relation between feldspatitic rocks and greisenization. In the Krušné hory/Erzgebirge, the greisens form the uppermost part of the cupolas. The interval about 200 m thick below the greisen is occupied by leucocratic mica-poor granite with individual layers of feldspatites in its deeper part (Jarchovský 2004). Within the feldspatites, facies with very different K/Na-ratio occur (K_2O 2–8 wt. %, Na_2O 3–8 wt. %). Non-altered Li-F granite occurs below the feldspatites. Feldspatization is a geologically younger or contemporaneous process than greisenization. In contrast, only Na-rich feldspatites were found in Dlhá dolina, forming the uppermost part of the cupola. Greisen stringers cut the albitite, which means that here the greisenization is somewhat younger than the origin of feldspar-rich rocks. Vertical zonality similar to that of the Dlhá dolina was described by Koval (1975) as typical for the so-called muscovite-albite type of rare-metal granites in the eastern parts of the former Soviet Union. Moreover, 40 years ago Koval (l.c.) interpreted the albite in Kazachstan and Transbaikalia as metasomatic supporting an earlier model established by Beus (e.g. Beus & Zalaškova 1962), but the overall zoning of plutons is conspicuously similar.

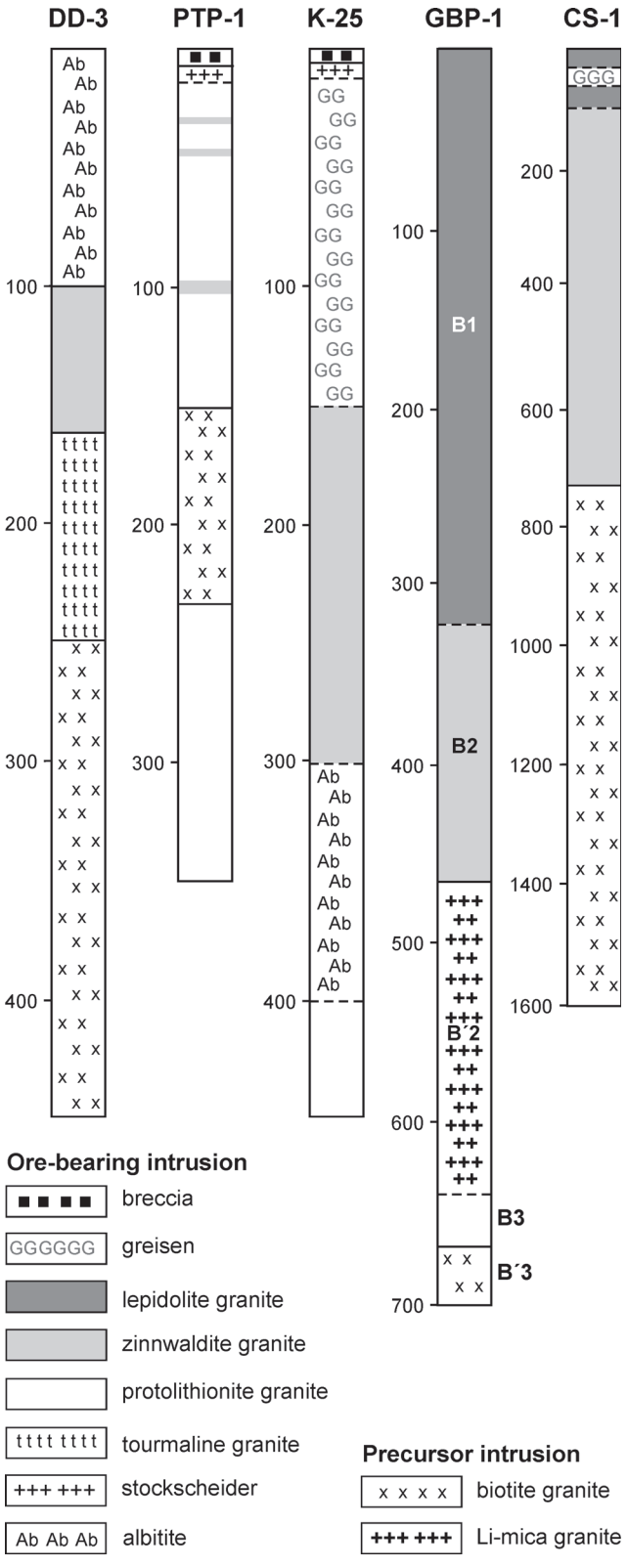

Fig. 9. Comparison of simplified vertical sections through different rare-metal granite plutons (see text for details). DD-3 Dlhá dolina, Slovakia (this work); PTP-3 Podlesí, Czech Republic (Breiter 2002); K-25 Krásno, Czech Republic (Jarchovský 1998); GBP-1 Beauvoir, France (Raimbault et al. 1995); CS-1 Cínovec, Czech Republic (Štemprok & Šulcek 1969).

The highly fractionated S-type granites of the Moldanubian and Saxothuringian zones of the European Variscides were formed during the Late Carboniferous: granites in the western and central Krušné hory/Erzgebirge at 318–327 Ma (Förster & Römmer 2010), granites in the Moldanubicum (southern Czech Republic and northern Austria) between 310–320 Ma (Scharbert 1998), and the Beauvoir granite in French Massif Central at 308 ± 2 Ma (Cheilletz et al. 1992). The early post-orogenic A-type rare-metal granites in the eastern Krušné hory/Erzgebirge is dated with still relatively large uncertainty into the broad interval of ca. 320–305 Ma (see Förster & Römmer (2010) and Breiter (2012) for discussion). The peraluminous Sn-bearing granites in Cornwall have distinctly younger–Late Permian date (274–293 Ma — Chen et al. 1993). The granites of the Gemeric Superunit, including the Dlhá dolina pluton, show only ~260 to 250 Ma age (Poller et al. 2002; Kohút & Stein 2005). Therefore they are probably the youngest tin-bearing granites found in the Variscan orogenic belt through the Europe, emplaced after termination of the Variscan orogeny. Moreover, the same age (262 ± 4 Ma) is found in the hypersolvus rift-related A-type granite from Turčok in the same Gemeric Superunit (Radvanec et al. 2009; Uher unpublished data). However, the Turčok granite shows different geochemical and mineralogical features in comparison to the Dlhá dolina granite: especially high Zr and REE but low Li, B, P, Sn, Ta and W contents as well as dissimilar REE and Nb phases, reflecting its metaluminous A-type character (Uher & Broska 1996; Broska & Uher 2001; Uher et al. 2009). Consequently, the Gemeric Permian S- and A-type granites do not represent an analogy with the Krušné hory/Erzgebirge area, where both fractionated S- and A-type members show enrichment in Li, Sn, B, Ta, and W (Breiter 2012).

Conclusions

In the Dlhá dolina pluton (DD-3 borehole), the primary character of contacts between different granite facies was strongly tectonically modified during Alpine (Cretaceous) thrusting; therefore, our interpretation concerning zoning, magma differentiation and evolution, despite all objective data, remains partly speculative. Nevertheless, taking into account all available information from the Dlhá dolina area and experience from better exposed ore-bearing plutons, we are able to formulate the following genetic scenario:

- Intrusion of common peraluminous magma formed a large body of biotite granites and intrusion of evolved peraluminous melt enriched in Li, P, F, Sn, Nb, Ta, and W took place;
- The evolved melt differentiated *in situ* forming three different rock types: tourmaline-Li-biotite granite at the bottom, topaz-zinnwaldite granite in the middle, and quartz albitite to albitite at the top. The composition of primary feldspar, micas, zircon and apatite document a relatively high degree of magmatic fractionation;
- A crucial part of Sn, Nb, and Ta crystallized from the melt as disseminated cassiterite and columbite within the albitite, while disseminated wolframite appears mainly within the topaz granite;

- Fluids separated from the last portion of crystallized magma (topaz-zinnwaldite granite) penetrated overlying albitite and resulted in small scale greisenization. Phosphorus from alkali feldspars was partially released forming secondary apatite. Disseminated bismuthinite originated at the same time;
- Much later, during Alpine thrusting, the upper part of the pluton was strongly tectonized and mylonitized along flat joins. Metamorphic Ca, Mg, and CO_2 rich fluids in neighbouring metacarbonates penetrated the fractured granite, forming thin carbonate veinlets and filling small cavities. These fluids also reacted with feldspars releasing the rest of the phosphorus from their crystal lattice, and forming Mg-rich mica varieties from magmatic and greisen micas. All bulk-rock and mineral markers were reset and now represent the *P-T* conditions of the Alpine overprint.

Acknowledgments: The granite samples were taken from the deposited DD-3 borehole in the storage house of the State Geological Institute of Dionýz Štúr on the basis of an official permit. We thank Mrs. Kateřina Švecová (Masaryk University Brno) for help with the cathodoluminescence analysis, Mr. Patrik Konečný and Mrs. Viera Kollárová (D. Štúr State Geological Institute, Bratislava) and Mrs. Zuzana Korbelová (Geological Institute CAS Praha) for assistance during electron-microprobe analyzing. Inspiring reviews by Igor Petrík and Milan Kohút are acknowledged. This investigation was supported by the Czech Science Foundation, Project Nos. P210/14/13600S and RVO 67985831, the VEGA Project No. 1/0257/13, and the APVV-0081-10 Project.

References

Bajaník Š., Ivanička J., Mello J., Pristaš J., Reichwalder P., Snopko L., Vozár J. & Vozárová A. 1984: Geological map of the Slovenské Rudohorie Mts. — eastern part 1:50,000. *D. Štúr Inst. Geol.*, Bratislava.

Baran J., Drnzíková L. & Mandáková K. 1970: Sn-W ore mineralization connected with the Hnilec granites. *Miner. Slovaca* 2, 159–165 (in Slovak).

Baran J., Drnzík E., Drnzíková L. & Mandáková K. 1971: Recent results of verification of Sn-W anomaly in Medvedí Potok. *Miner. Slovaca* 3, 151–153 (in Slovak).

Bastos Neto A.C., Pereira V.P., Ronchi L.H., De Lima E.F. & Frantz J.C. 2009: The world-class Sn, Nb, Ta, F (Y, REE, Li) deposit and the massive cryolite associated with the albite-enriched facies of the Madeira A-type granite, Pitinga Mining District, Amazonas State, Brazil. *Canad. Mineralogist* 47, 1329–1357.

Beus A.A. & Zalaškova N.E. 1962: High-temperature postmagmatic metasomatism in granitoids. *Izvestiya AN SSSR, Ser. Geol.*, 13–31 (in Russian).

Breiter K. 2002: From explosive breccia to unidirectional solidification textures: magmatic evolution of a phosphorus- and fluorine-rich granite systém (Podlesí, Krušné hory Mts., Czech Republic). *Bull. Czech Geol. Surv.* 77, 67–92.

Breiter K. 2012: Nearly contemporaneous evolution of the A- and S-type fractionated granites in the Krušné hory/Erzgebirge Mts., Central Europe. *Lithos* 151, 105–121.

Breiter K. & Kronz A. 2004: Phosphorus-rich topaz from fractionated granites (Podlesí, Czech Republic). *Miner. Petrology* 81, 235–247.

Breiter K., Förster H. & Seltmann R. 1999: Variscan silicic magmatism and related tin-tungsten mineralization in the Erzgebirge-Slavkovský les metamollgenic province. *Mineralium Depos.* 34, 505–521.

Breiter K., Frýda J. & Leichmann J. 2002: Phosphorus and rubidium in alkali feldspars: case studies and possible genetic interpretation. *Bull. Czech Geol. Surv.* 77, 93–104.

Breiter K., Škoda R. & Uher P. 2007: Nb-Ta-Ti-W-Sn-oxide minerals as indicator of a peraluminous P- and F-rich granitic system evolution: Podlesí, Czech Republic. *Miner. Petrology* 91, 225–248.

Breiter K., Müller A., Leichmann J. & Gabašová A. 2005: Textural and chemical evolution of a fractionated granitic system: the Podlesí stock, Czech Republic. *Lithos* 80, 323–345.

Broska I. & Uher P. 2001: Whole-rock chemistry and genetic typology of the West-Carpathian Variscan granites. *Geol. Carpathica* 52, 79–90.

Cheilletz A., Archibald D.A., Cuney M. & Charoy B. 1992: Ages $^{40}Ar/^{39}Ar$ du leucogranite a topaze-lepidolite de Beauvoir et des pegmatites sodolithiques de Chédeville (Nord du Massif Central, France). Significance pétrologique et géodynamique. *C. R. Acad. Sci.* 315, 326–336.

Chen Y., Clark A.H., Farrar E., Wasteneys H.A.H.P., Hodgson M.J. & Bromley A.V. 1993: Diachronous and independent histories of plutonism and mineralization in the Cornubian Batholith, southwest England. *J. Geol. Soc.* 150, 1183–1191.

Dianiška I., Breiter K., Broska I., Kubiš M. & Malachovský P. 2002: First phosphorus-rich Nb-Ta-Sn-specialised granite from the Carpathians Dlhá dolina valley granite pluton, Gemeric Superunit. *Geol. Carpathica, Spec. Issue*, 53 (CD-ROM).

Drnzíková L., Drnzík E., Mandáková K. & Baran J. 1975: Criteria of tin and metallogenetic specialization of some granite types of the Spiš-Gemer Ore Mountains. *Miner. Slovaca* 7, 53–59 (in Slovak).

Förster H.J. & Römmer R.L. 2010: Carboniferous magmatism. In: Linnemann U. & Romer R.L. (Eds.): Pre-Mesozoic geology of Saxo-Thuringia — from the Cadomian active margin to the Variscan orogen. *Schweizerbart. Stuttgart*, 287–308.

Frolov A.A. 1978: Mineral deposits in stockworks. *Nauka*, Moskva, 1–264 (in Russian).

Haapala 1995: Metallogeny of the Rapakivi granites. *Miner. Petrology* 54, 149–160.

Hösel G. (Ed.) 1994: Das Zinnerz-Lagerstattengebiet Ehrenfriedersdorf/Erzgebirge. *Bergbau in Sachsen,* 1, *LFuB*, Freiberg, 1–195.

Jahns R.H. 1955: The study of pegmatites. *Econ. Geol.* 50, 1025–1130.

Jarchovský T. 1998: Sn-W mineralization in the Krásno district. In: Breiter K. (Ed.): Genetic significance of phosphorus in fractionated granites — Excursion guide. *Czech Geol. Surv.*, Praha, 77–92.

Jarchovský T. 2004: The nature and genesis of greisen stocks at Krásno, Slavkovský les area — Western Bohemia, Czech Republic. *J. Czech Geol. Soc.* 51, 201–216.

Kilík J. 1997: Geological characteristic of the talc deposit in Gemerská Poloma–Dlhá dolina. *Acta Montanistica Slovaca* 2, 71–80 (in Slovak).

Kohút M. & Stein H. 2005: Re-Os molybdenite dating of granite-related Sn-W-Mo mineralisation at Hnilec, Gemeric Superunit, Slovakia. *Miner. Petrology* 85, 117–129.

Koval P.V. 1975: Petrology and geochemistry of albitized granites. *Nauka*, Moskva, 1–258 (in Russian).

Kovalenko V.I. & Kovalenko N.I. 1976: Ongonites (topaz-bearing quartz keratophyre) — subvolcanic analoques of rare-metal Li-F granites. *Nauka*, Moskva, 1–124 (in Russian).

Kubiš M. & Broska I. 2005: Role of boron and fluorine in evolved granitic rock systems (on example Hnilec area, Western Carpathians). *Geol. Carpathica* 56, 193–204.

Kubiš M. & Broska I. 2010: The granite system near Betliar village (Gemeric Superunit, Western Carpathians): evolution of a composite silicic reservoir. *J. Geosci.* 55, 131–148.

Küster D. 2009: Granitoid-hosted Ta mineralization in the Arabian-Nubian Shield: Ore deposit types, tectono-metallogenetic setting and petrogenetic framework. *Ore Geol. Rev.* 35, 68–86.

Lehmann B. 1990: Metallogeny of tin. Lecture notes in earth sciences. *Springer*, Heidelberg-Berlin 32, 1–211.

London D. 2014: A petrologic assessment of internal zoning in granitic pegmatites. *Lithos* 184–187, 74–104.

London D., Morgan G.B. VI, Babb H.A. & Loomis J.L. 1993: Behaviour and effects of phosphorus in the system Na_2O–K_2O–Al_2O_3–SiO_2–P_2O_5–H_2O at 200 MPa (H_2O). *Contr. Mineral. Petrology* 113, 450–465.

Losos Z. & Vižda P. 2006: Mineralogy and genesis of the cassiterite from Kovářová near Nedvědice. [Sborník mineralogie Českého masívu a Západních Karpat]. *University of Palacky in Olomouc*, 30–40 (in Czech). ISBN 80-244-1560-7.

Malachovský P., Turanová L. & Dianiška I. 1992: Final report on mineral exploration from Gemerská Poloma. *Unpubl. report*, *Geofond archive*, Bratislava, 1–180 (in Slovak).

Malachovský P., Dianiška I., Matula I., Kamenický J., Kobulský J., Hodermarský J., Fabian M., Radvanec M., Kozáč J., Vlasák M., Mihalič A., Ščerbáková A., Seliga J. & Novoveský M. 1983: SGR — high temperature mineralization — Sn, W, Mo ores. *Unpubl. report*, *Geofond archive*, Bratislava, 1–248 (in Slovak).

McDonough F.V. & Sun S. 1995: The composition of the Earth. *Chem. Geol.* 120, 223–253.

Němec D. & Páša J. 1986: Regionally metamorphosed greisens of the Moldanubicum. *Mineralium Depos.* 21, 12–21.

Petrasová K., Faryad S.W., Jeřábek P. & Žáčková E. 2007: Origin and metamorphic evolution of magnesite-talc adjacent rocks near Gemerská Poloma, Slovak Republic. *J. Geosci.* 52, 125–132.

Petrík I., Kubiš M., Konečný P., Broska I. & Malachovský P. 2011: Rare phosphates from the Surovec topaz-Li-mica microgranite, Gemeric unit, Western Carpathians, Slovakia: the role of the F/H_2O in the melt. *Canad. Mineralogist* 49, 521–540.

Petrík I., Čík Š., Miglierini M., Vaculovič T., Dianiška I. & Ozdín D. 2014: Alpine oxidation of lithium micas in Permian S-type granites (Gemeric unit, Western Carpathians, Slovakia). *Mineral. Mag.* 78, 507–533.

Plašienka D., Broska I., Kissová D. & Dunkl I. 2007: Zircon fission-track dating of granites from the Vepor-Gemer-Belt (Western Carpathians): constraints for the Early Alpine exhumation history. *J. Geosci.* 52, 113–123.

Poller U., Uher P., Broska I., Plašienka D. & Janák M. 2002: First Permian–Early Triassic zircon ages for tin-bearing granites from the Gemeric unit (Western Carpathians, Slovakia): connection to the post-collisional extension of the Variscan orogen and S-type granite magmatism. *Terra Nova* 14, 41–48.

Radvanec M., Koděra P. & Prochaska W. 2004: Mg replacement at the Gemerská Poloma talc-magnasite deposit, Western Carpathians, Slovakia. *Acta Petrol. Sin.* 20, 773–790.

Radvanec M., Konečný P., Ondrejka M., Putiš M., Uher P. & Németh Z. 2009: The Gemeric granites as an indicator of the crustal extension above the Late-Variscan subduction zone and during the Early Alpine riftogenesis (Western Carpathians): An interpretation from the monazite and zircon ages dated by CHIME and SHRIMP methods. *Miner. Slovaca* 41, 381–394 (in Slovak with English resumé).

Raimbault L., Cuney M., Azencott C., Duthou J.L. & Joron J.L. 1995: Geochemical evidence for a multistage magmatic genesis of Ta-Sn-Li mineralization in the granite at Beauvoir, French Massif Central. *Econ. Geol.* 90, 548–596.

Scharbert S. 1998: Some geochronological data from the South Bohemian Pluton in Austria: a critical review. *Acta Univ. Carolinae Geol.* 42, 114–118.

Seltmann R., Kampf H. & Möller P. (Eds.) 1994: Metallogeny of collisional orogens. *Czech Geol. Surv.*, Praha, 1–448.

Solomovich L.I., Trifonov B.A. & Sabelnikov S.E. 2012: Geology and mineralization of the Uchkoshkon tin deposit associated with a breccia pipe, Eastern Kyrgyzstan. *Ore Geol. Rev.* 44, 59–69.

Štemprok M. 1993: Genetic models for metallogenic specialization of tin and tungsten deposits associated with the Krušné hory-Erzgebirge granite batholith. *Res. Geol., Spec. Issue* 15, 373–383.

Štemprok M. & Šulcek Z. 1969: Geochemical profile through an ore-bearing lithium granite. *Econ. Geol.* 64, 392–404.

Štemprok M., Novák J.K. & David J. 1994: The association between granites and tin-tungsten mineralization in the Krušné hory (Erzgebirge), Czech Republic. *Monograph, Ser., Mineral Depos.* 31, 97–129.

Taylor R.P. & Strong D.F. (Eds.) 1985: Recent advances in the geology of granite-related mineral deposits. *Canad. Inst. Mining and Metallurgy, Spec. Vol.*, Montreal 39, 1–445.

Tischendorf G. (Ed.) 1989: Silicic magmatism and metallogenesis of the Erzgebirge. *Veröff. Zentralinst. f. Physik d. Erde,* Potsdam 107, 1–316.

Tischendorf G., Gottesmann B. & Förster H.-J. 1999: The correlation between lithium and magnesium in trioctahedral micas: Improved equations for Li_2O estimation from MgO data. *Mineral. Mag.* 63, 57–74.

Tréger M. & Matula I. 1977: New inditions of tin ore mineralization in the Spiš-Gemer Ore Mountains and perspectives of their prospecting. *Geol. Průzkum* 19, 262–265.

Uher P. & Broska I. 1996: Post-orogenic Permian granitic rocks in the Western Carpathian-Pannonian area: Geochemistry, mineralogy and evolution. *Geol. Carpathica* 47, 311–321.

Uher P., Ondrejka M. & Konečný P. 2009: Magmatic and post-magmatic Y-REE-Th phosphate, silicate and Nb-Ta-Y-REE oxide minerals in A-type metagranite: an example from the Turčok massif, the Western Carpathians, Slovakia. *Mineral. Mag.* 73, 1009–1025.

Vozárová A., Šarinová K., Larionov A., Presnyakov S. & Sergeev S. 2010: LateCambrian/Ordovician magmatic arc type volcanism in the Southern Gemericum basement, Western Carpathians, Slovakia: U-Pb (SHRIMP) data from zircons. *Int. J. Earth Sci.* 99 (*Suppl 1*), S17–S37.